



Research

Cite this article: Subramaniyam NP, Donges JF, Hyttinen J. 2015 Signatures of chaotic and stochastic dynamics uncovered with ε -recurrence networks. *Proc. R. Soc. A* **471**: 20150349. <http://dx.doi.org/10.1098/rspa.2015.0349>

Received: 28 May 2015

Accepted: 2 October 2015

Subject Areas:

applied mathematics, graph theory

Keywords:

time-series analysis, complex networks, chaotic dynamics, stochastic dynamics

Author for correspondence:

N. P. Subramaniyam

e-mail: npsubramaniyam@gmail.com

Electronic supplementary material is available at <http://dx.doi.org/10.1098/rspa.2015.0349> or via <http://rspa.royalsocietypublishing.org>.

Signatures of chaotic and stochastic dynamics uncovered with ε -recurrence networks

N. P. Subramaniyam^{1,2}, J. F. Donges^{3,4}

and J. Hyttinen^{1,2}

¹Department of Electronics and Communications Engineering, Tampere University of Technology, Tampere, Finland

²BioMediTech, Tampere, Finland

³Earth System Analysis, Potsdam Institute for Climate Impact Research, Potsdam, Germany

⁴Planetary Boundary Research Lab, Stockholm University, Stockholm, Sweden

An old and important problem in the field of nonlinear time-series analysis entails the distinction between chaotic and stochastic dynamics. Recently, ε -recurrence networks have been proposed as a tool to analyse the structural properties of a time series. In this paper, we propose the applicability of local and global ε -recurrence network measures to distinguish between chaotic and stochastic dynamics using paradigmatic model systems such as the Lorenz system, and the chaotic and hyper-chaotic Rössler system. We also demonstrate the effect of increasing levels of noise on these network measures and provide a real-world application of analysing electroencephalographic data comprising epileptic seizures. Our results show that both local and global ε -recurrence network measures are sensitive to the presence of unstable periodic orbits and other structural features associated with chaotic dynamics that are otherwise absent in stochastic dynamics. These network measures are still robust at high noise levels and short data lengths. Furthermore, ε -recurrence network analysis of the real-world epileptic data revealed the capability of these network measures in capturing dynamical transitions using short window sizes. ε -recurrence network analysis is a powerful method in uncovering the signatures of chaotic and stochastic dynamics based on the geometrical properties of time series.

1. Introduction

Distinguishing chaotic from stochastic processes is an important problem arising in many fields ranging from biology and physics to ecology and finance. In this paper, we propose an approach based on ε -recurrence networks [1], obtained by transforming time series into complex networks, to distinguish between chaotic and stochastic dynamics. Numerous approaches have been proposed to solve this critical issue of distinguishing between stochastic and chaotic dynamics, which is faced with several challenges, because both chaotic and stochastic processes share some common properties, for example, a broadband power spectrum, delta-like autocorrelation function and long-term irregular behaviour [2,3]. It may even be practically impossible to distinguish high-dimensional chaos from a stochastic process. Because in a chaotic system, the time evolution of two nearby trajectories will diverge exponentially fast compared with a stochastic system where the separation is randomly distributed [4], methods based on short-term predictability have been applied to distinguish chaos from noise [5,6]. Thus, for a chaotic time series, the accuracy of forecast should decrease with increasing prediction-time interval and for a stochastic time series this accuracy should be independent of the prediction-time interval [6]. Kaplan & Glass [7,8] proposed a test for determinism based on the measurement of average directional vectors in a coarse-grained phase space. This test is based on the observation that the tangents to the trajectories of a deterministic system, passing through a small region in phase space, will be well aligned, that is, oriented in the same direction, a behaviour not observed in stochastic dynamics [7,8]. Another line of approach borrows from the concept that a chaotic attractor should have finite, non-integer values for fractal dimensions, whereas stochastic processes must theoretically exhibit infinite dimensions. This traditional view was challenged by Osborne & Provenzale [9], when they demonstrated that finite correlation dimension could be obtained from a simple class of coloured random noise characterized by power-law spectra. Recently, quantifiers from information theory have been used to address the issue of distinguishing between chaotic and stochastic dynamics, leading to some interesting results [10]. Rosso *et al.* [3] introduced the complexity–entropy (C–E) causality plane, a two-dimensional representation space that relates the two information theoretic quantities namely entropy and complexity, to distinguish between stochastic and chaotic dynamics. By explicitly including the time-scale notion, Zunino *et al.* [2] proposed the multiscale C–E plane to identify the time scales at which stochastic and chaotic components govern the system’s dynamics. The classification of the stochastic or chaotic character of a given time series at different resolution scale using entropic analysis was first proposed by Cencini *et al.* [11]. Olivares *et al.* [12,13] also proposed a combination of two information theoretic quantities, the Shannon entropy and the Fisher information, to obtain the Shannon–Fisher causality ($S \times F$) plane and showed that stochastic and chaotic dynamics map to different locations on this two-dimensional plane.

By bridging the gap between nonlinear time-series analysis and complex network theory, methods to transform a time series into a complex network comprising nodes which represent the state vectors in phase space and edges that are defined based on some criteria such as mutual closeness or transition probabilities, have emerged [14,15]. Different classes of such time-series-based complex networks exist such as proximity networks [1,14,16–18], transition networks [19] or visibility graphs [20,21]. A comprehensive review on these network types is given elsewhere [14]. The underlying principle in this approach is to characterize the topology of the resultant network using tools from graph theory to gain insights into the dynamics underlying the time series. Complex network-based univariate and multivariate time-series analysis has been successfully applied in different fields, including climatology [1,15,22] fluid dynamics [23–26] and neuroscience [27–30], to cite a few.

Lacasa & Toral [4] used horizontal visibility graphs (HVGs) [31], a geometrically simpler version of the visibility graph algorithm, to distinguish between chaotic and stochastic (correlated and uncorrelated) dynamics based on the node degree distribution (specifically the slope of the logarithm of the degree distribution) of the resultant networks. Recently, Ravetti *et al.* [10]

showed that the HVG approach is sensitive to the scaling zone and combined the HVG approach with information theory quantifiers (the $\mathcal{S} \times \mathcal{F}$ plane) that leads to a better characterization of deterministic and stochastic dynamics.

Recurrence is a fundamental property of dynamical systems [32] and using the recurrence matrix derived from a time series, one can define a recurrence network by reinterpreting the recurrence matrix as an adjacency matrix of a complex, undirected network [1,14]. Xu *et al.* [33] first proposed the concept of transforming a time series into an undirected complex network. Such networks, known as recurrence networks, belong to the class of proximity networks where the existence of an edge in the network is defined based on the mutual closeness between two state vectors (nodes). Because such a recurrence matrix can be defined in many ways, depending on the chosen neighbourhood criteria, there are different types of recurrence networks [14], namely k -nearest neighbour recurrence networks [18,34], adaptive nearest neighbour recurrence networks [33] and ε -recurrence networks [1,14]. Specifically, the neighbourhood can be defined in terms of either a fixed number of edges (k -nearest or adaptive nearest neighbour recurrence networks) [18,33–35] or fixed phase space distance (ε -recurrence networks) centred around a node i (i.e. a state vector in phase space) [1]. All the nodes that fall within this volume are connected to the node i by forming an edge. ε -recurrence networks are both symmetric and undirected. In this work, we will be dealing only with ε -recurrence networks.

Over recent years, ε -recurrence networks have gained much popularity and they have been thoroughly analysed and applied using data from simulated as well as real-world systems. Using model systems, Donner *et al.* [14] studied the ε -dependence of local and global network properties. Donges *et al.* [36] provided a thorough analytical framework for ε -recurrence network analysis of periodic/quasi-periodic dynamics, chaotic maps, stochastic processes and higher-dimensional symmetric sets. Zou *et al.* [37] showed that global network measures such as global clustering coefficient C and average path length \mathcal{L} derived from ε -recurrence networks can be used to distinguish between periodic and chaotic dynamics in both discrete and continuous-time dynamical systems. Furthermore, using the Rössler system, they showed that these network measures can reliably identify complex periodic windows in parameter space. Because a ε -recurrence network can be considered as a random geometric graph, the distribution of the nodes in the space where the network is embedded is determined by the probability density function of the system's invariant measure [36]. Furthermore, the edges are formed only between those nodes that are spatially close to each other as determined by some distance threshold. Thus, based on the theory of random geometric graphs [38], Donner *et al.* [39] provided the relationship between geometric properties of a dynamical system and the transitivity properties such as the local clustering coefficient and transitivity of the associated ε -recurrence networks. Specifically, it was shown that these transitivity measures can be considered as an alternative notion of fractal dimension of the dynamical system under study [39]. Also, it has been demonstrated that the ε -recurrence networks display power-law degree distributions and the scaling exponent of the degree distribution is related to system's invariant density [37]. It has also been demonstrated that the transitivity properties can reliably detect unstable periodic orbits (UPOs) in model systems [14].

Because transitivity properties can be understood as some notion of fractal dimension, the associated transitivity dimension should exhibit non-integer values for dissipative chaotic systems. This feature could be particularly useful in distinguishing whether the observed dynamics is chaotic or stochastic. Thus, in the case of a stochastic process (which theoretically exhibits infinite dimensions), the estimated dimension should be limited by the phase space dimension. Characterizing and differentiating a chaotic process from a stochastic process based on the transitivity dimension has not been studied so far. It was shown by Donges *et al.* [36] that ε -recurrence network measures cannot distinguish between stochastic and deterministic process if both have identical invariant density distribution in phase space. This observation was based on the analytical computation of continuous ε -recurrence network measures—transitivity, clustering coefficient, average path length and betweenness for the one-dimensional Bernoulli map and uniform noise. This observation, as mentioned by the authors themselves, holds true when

embedding is not used and it has been proposed that an additional embedding can overcome this shortcoming [14]. One reason for this could be the difference in the structure of chaotic attractors, primarily owing to the presence of densely packed UPOs, compared with time-delay embedded stochastic processes which fail to recover this structure. However, this has not been studied or tested elaborately using well-known model systems. Thus, we hypothesize that the transitivity dimension of the chaotic attractors should be lower than that of stochastic dynamics, which should have a transitivity dimension close to the embedding dimension. Previously, we have shown that by combining ε -recurrence network measures with iterative amplitude adjusted Fourier transform (iAAFT) surrogates [40] which represent stationary, linearly correlated, stochastic processes (coloured Gaussian), different classes of electroencephalography (EEG) data can be distinguished [28]. Particularly, we observed that the rejection rate of the null hypothesis based on iAAFT surrogates for the network measures global clustering coefficient C and average path length L was higher for pathological EEG compared with normal EEG [28]. However, a rigorous evaluation of the ability of ε -recurrence network measures to particularly distinguish deterministic from stochastic processes and of how embedding alters the phase space distribution of these processes is missing. Also, a careful consideration of the effects of noise on the recurrence networks to distinguish between stochastic and chaotic processes and the impact of data length on such distinction has not been addressed so far. In particular, detecting and distinguishing chaotic from stochastic processes could pose great challenges when the data is short and noisy. Because an important advantage of network-based time-series analysis is that network measures can be reliably estimated from rather short time series with high confidence, we hypothesize that such an approach could be particularly useful in addressing this challenge compared with other classical approaches of nonlinear time-series analysis.

Using ε -recurrence networks constructed from stochastic and chaotic dynamics, we investigate the applicability of global measures—transitivity dimension, assortativity, average path length and the vertex-based measures—local clustering coefficient, betweenness centrality, closeness centrality and degree centrality in distinguishing deterministic (chaos) processes from stochastic processes. As an example of low and high dimensional chaotic systems, we use Lorenz, chaotic Rössler and four-dimensional Rössler systems, respectively. Specifically, we use the x -component of these systems and the corresponding iAAFT surrogates (stochastic, linearly correlated process, sharing the power spectrum and amplitude distribution with the original chaotic time series) derived from the x -component to construct ε -recurrence networks representing chaotic and stochastic dynamics, respectively. We construct the ε -recurrence networks representing chaotic and stochastic dynamics for varying embedding dimensions and recurrence rates (related to the threshold ε). Additionally, we also investigate the effect of increasing noise levels and data length on the network measures and their distributions (in the case of vertex-based measures) for ε -recurrence networks derived from chaotic dynamics. We compare our results with the C–E plane approach proposed in reference [3]. In addition to the above-described theoretical simulation, we also present the results from the application of ε -recurrence network analysis to epileptic EEG data, which contains pre-seizure, seizure and post-seizure segments. Here, we investigate if ε -recurrence network measures, when applied to rather short window-sizes can track dynamical changes underlying such real-world, noisy biological signals.

2. Recurrence networks and measures

(a) Recurrence networks

Given a phase space vector, a recurrence matrix can be defined as [32]

$$R(i,j) = \Theta(\varepsilon - \|x_i - x_j\|), \quad (2.1)$$

where ε is a predefined global threshold, x_i and x_j are the m -dimensional phase space vectors at time t_i and t_j (with $t_j < t_i$), respectively, and $\Theta(\cdot)$ is the Heaviside function. If only the univariate time series is available, then one can reconstruct the phase space vector using time-delay

embedding [41], $\mathbf{x}_i = (x(t_i), x(t_i - \tau), \dots, x(t_i - (m - 1)\tau))$. Here, m is the embedding dimension and τ is the optimal time lag that can be determined using standard methods such as false nearest neighbour and first minimum of automutual information function, respectively [42].

One can define an adjacency matrix A of a recurrence network using the recurrence matrix defined above as follows [1]

$$A(i, j) = R(i, j) - \delta(i, j), \quad (2.2)$$

where $\delta(i, j)$ is the Kronecker delta, introduced to avoid artificial self-loops [32]. Each vertex i of a recurrence network represents a state vector \mathbf{x}_i and the edges between the nodes are formed based on their mutual closeness as defined by euclidean or Manhattan or maximum norm. Note that owing to the way recurrence networks are formed, they can be considered as random geometric graphs [36]. In this work, we use the maximum norm as the distance norm. Furthermore, instead of fixing ε , we fix the recurrence rate $RR = (1/N^2) \sum_{i,j=1}^N R(i, j)$, where N is the number of state vectors, because we are essentially interested in comparing the properties of systems (chaotic and stochastic) with different phase space diameters [14]. Thus, we vary RR from 0.01 to 0.05 in steps of 0.01. Additionally, we also vary the embedding dimension m from 1 to 5.

(b) Recurrence network measures

(i) Degree centrality

Degree centrality of a vertex i can be defined as the number of vertices directly connected to i . It is given as

$$k_i = \sum_{j=1}^N A(i, j). \quad (2.3)$$

This measure can be normalized to yield the local connectivity, which describes the local phase space density [14], that is, the local recurrence rate

$$\rho_i = \frac{k_i}{N - 1}, \quad (2.4)$$

where N is the data length (or the number of embedded state vectors).

(ii) Closeness centrality

Closeness centrality can be defined as the inverse of the average geodesic distance (i.e. the length of the shortest path) between a vertex i and all other vertices in a network. According to this definition, a vertex is considered central, if it is close to all the other vertices in the network. Let $d(i, j)$ be the shortest-path length between two vertices i and j . The closeness centrality of the vertex i is then defined as [43]

$$c_i = \frac{N - 1}{\sum_{j=1}^N d(i, j)}. \quad (2.5)$$

Other definitions for the closeness centrality exist. For instance, in reference [44], c_i is simply defined as the inverse of $\sum_{j=1}^N d(i, j)$, without the factor $N - 1$ and sometimes, it is also defined as the mean geodesic distance between a vertex i and all other vertices in a network. In this work, we adapt the definition given in equation (2.5). For a recurrence network, closeness centrality gives the local centeredness of a state in the phase space and with a small number of ε -jumps, most of the vertices are reachable from a vertex with high centrality [14].

(iii) Betweenness centrality

Betweenness centrality, like other centrality measures, also describes the importance of a vertex in a network and was first introduced in references [45,46]. The betweenness centrality of a vertex i is defined as the total number of the fraction of shortest paths between all pairs of vertices that pass through i . Let σ_{jk} be the total number of shortest paths from a vertex j to k in a network and

$\sigma_{jk}(i)$ be the number of short paths (from a total of σ_{jk}) that pass through vertex i . The betweenness centrality for a vertex i can be defined as [47]

$$b_i = \sum_{j \neq i \neq k} \frac{\sigma_{jk}(i)}{\sigma_{jk}}. \quad (2.6)$$

When this measure is applied to a recurrence network, where the vertices represent the states of a dynamical system, a high value of betweenness is acquired by those vertices belonging to a sparse region in phase space that separates different high-density clusters [14].

(iv) Local clustering coefficient

The local clustering coefficient for a vertex i gives the probability that two randomly drawn neighbours j and q are themselves neighbours. In an undirected graph, because the maximum possible number of connections between the neighbours of a vertex i is given as $k_i(k_i - 1)/2$, the local clustering coefficient can be given by the ratio

$$c_i = \frac{\sum_{j,q} A(i,j)A(j,q)A(q,i)}{k_i(k_i - 1)}. \quad (2.7)$$

(v) Transitivity dimension

Network transitivity measures the fraction of the connected triples in a network that form triangles, where a connected triple is defined as a single vertex connected to an unordered pair of vertices [48]. It was first introduced in reference [49]. It can be given by the following ratio

$$\mathcal{T} = \frac{\sum_{i,j,q=1}^N A(i,j)A(j,q)A(q,i)}{\sum_{i,j,q=1}^N A(i,j)A(q,i)}. \quad (2.8)$$

Essentially, \mathcal{T} also measures the probability that if two vertices are neighbours of another vertex, then the two vertices themselves are neighbours. This definition is similar to the notion of clustering coefficient, but there is a slight difference between these two measures. While the averaged network clustering coefficient is the mean, computed over all vertices, of the ratio given in equation (2.7), the network transitivity is the ratio of the mean number of edges between the neighbours of a vertex and the mean number of possible edges between neighbours of a vertex [49]. Also, network transitivity gives equal weight to all triangles in a network. In reference [39], a new measure of global dimensionality of a set of points known as transitivity dimension was introduced, which can be considered as some notion of fractal dimension. The transitivity dimension at a single-scale ε is given as [39]

$$D_{\mathcal{T}_\varepsilon} = \frac{\log \mathcal{T}}{\log(3/4)}. \quad (2.9)$$

For the sake of simplicity, in the remainder of this paper, we always refer to single-scale transitivity dimension as *transitivity dimension*, $D_{\mathcal{T}}$.

(vi) Assortativity

A network is said to be assortative if vertices of similar degrees tend to link up with each other. The measure assortativity can be defined as a Pearson product-moment correlation of the vertex degrees on either ends of all the edges [50]

$$\mathcal{R} = \frac{(1/N) \sum_{j>i} k_i k_j A(i,j) - [(1/N) \sum_{j>i} (1/2)(k_i + k_j) A(i,j)]^2}{(1/N) \sum_{j>i} (1/2)(k_i^2 + k_j^2) A(i,j) - [(1/N) \sum_{j>i} (1/2)(k_i + k_j) A(i,j)]^2}. \quad (2.10)$$

A recurrence network show assortative mixing implies that the density of states change more slowly and continuously and, hence, \mathcal{R} can be considered as a measure of the fragmentation of the attractor [14].

(vii) Average path length

The average path length \mathcal{L} for a graph can be defined as the mean value of geodesic lengths over all pairs of nodes. It is given as

$$\mathcal{L} = \frac{1}{N(N-1)} \sum_{i \neq j} d(i,j). \quad (2.11)$$

The disconnected pairs of nodes are not included in computing the average [1,51]. Dynamical transitions in complex systems can be identified by changes in the values of \mathcal{L} [1,22,52,53]. For example, a continuous dynamical system with periodic trajectory has a higher \mathcal{L} compared with a system exhibiting chaotic dynamics for comparable ε [37].

3. Simulations and results

(a) Model systems

In this study, we consider the Lorenz system [54],

$$\dot{x} = 10(y - x), \quad \dot{y} = x(28 - z), \quad \dot{z} = xy - \frac{8}{3}z, \quad (3.1)$$

and the chaotic Rössler system [55],

$$\dot{x} = -y - z, \quad \dot{y} = x + 0.1y, \quad \dot{z} = 0.1 + z(x - 18), \quad (3.2)$$

as examples for three-dimensional chaotic oscillators. We also consider the hyper-chaotic Rössler system [56],

$$\dot{x} = -y - z, \quad \dot{y} = x + 0.25y + w, \quad \dot{z} = 3 + xz, \quad \dot{w} = -0.5z + 0.05w. \quad (3.3)$$

In each case, we consider the x -component of the system and reconstruct the dynamics for varying embedding dimension using the method of delays. The optimal embedding lag in each case was found using the auto mutual information criterion [57]. We obtained $\tau = 3, 28$, and 107 for the x -component of the Lorenz, chaotic Rössler and hyper-chaotic Rössler systems, respectively. For the (hyper-) chaotic systems, we generated $N = 100\,000$ data points (after discarding initial 50 000 points as transients) with step size of 0.05 (for Lorenz and chaotic Rössler) and 0.015 (for hyper-chaotic Rössler). We then randomly choose $N = 200, 500, 1000, 5000$ and 10 000 points as a sample of state vectors from the chaotic attractor [58]. In the case of the hyper-chaotic attractor, we used $N = 10\,000, 15\,000$ and 20 000. Furthermore, to study the effect of noise, we generated 100 realizations from the above-described chaotic systems, for various data lengths. We added observational noise to the x -component of each system

$$x_{\text{noise}}(t) = x(t) + \eta(t), \quad (3.4)$$

where $\eta(t) \sim \mathcal{WN}(0, \sigma^2)$. Here, \mathcal{W} is defined as the level of noise, which is given as a percentage of the standard deviation of the noise-free data $x(t)$. We added Gaussian noise at levels 10%, 20%, 40%, 60% and 100%. We also generated 99 iAAFT surrogates in each case using the x -component.

(b) Global network measures

Figures 1–3 show the variation of D_T , \mathcal{L} and \mathcal{R} with respect to the embedding dimension m for different RR, for the chaotic and stochastic dynamics reconstructed from the x -component of the Lorenz system and its iAAFT surrogates, respectively. It can be seen from figure 1 that D_T for the Lorenz attractor (chaotic dynamics) saturates at a fractal dimension <2 (it varies approximately between 1.5 for RR = 0.05–1.8 for RR = 0.01), whereas in the case of the stochastic dynamics, the D_T continues to increase with the embedding dimension m , consistent with the theory (see §1). The classical measures, correlation dimension and the upper box-counting dimension, which theoretically represent respectively the upper and lower bounds of the fractal dimension of a dynamical system, were estimated to be 2.06 and 2.33, respectively, for a Lorenz system [59].

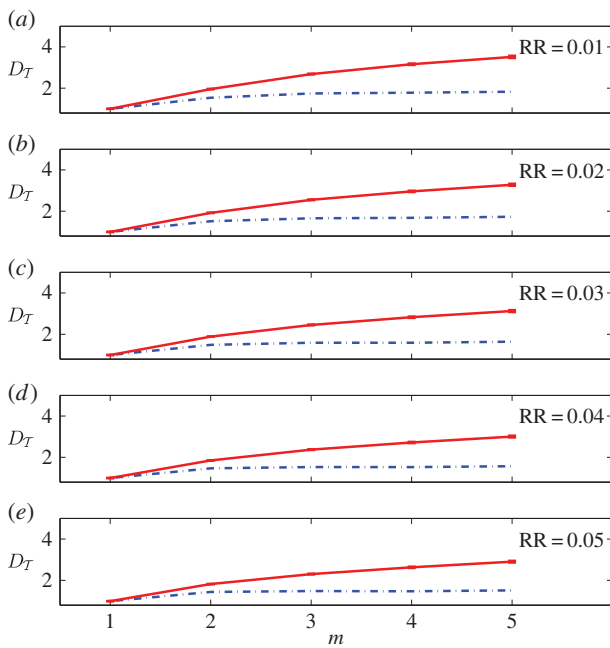


Figure 1. Transitivity dimension D_T of the ε -recurrence networks constructed from the x -component of Lorenz system (dashed blue lines) and corresponding iAAFT surrogates (solid red lines) for varying embedding dimension m and recurrence rate RR ($N = 10\,000$). The D_T for surrogates are averaged over 100 realizations with error bars representing the standard deviation. (Online version in colour.)

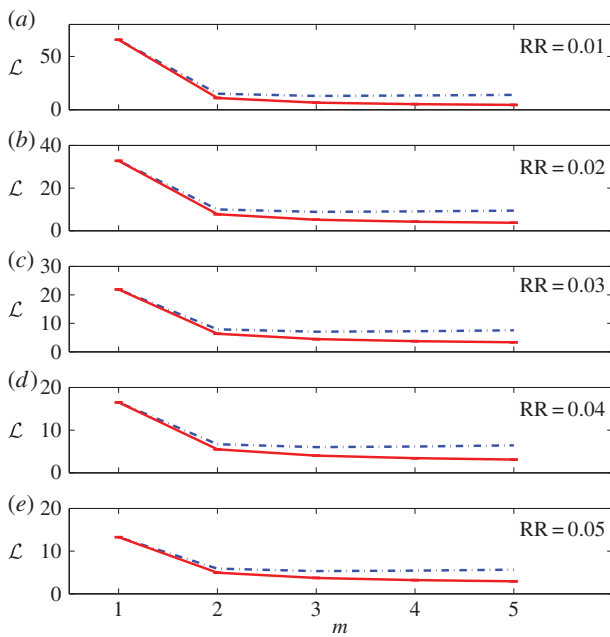


Figure 2. Average path length \mathcal{L} of the ε -recurrence networks constructed from the x -component of Lorenz system (dashed blue lines) and corresponding iAAFT surrogates (solid red lines) for varying embedding dimension m and recurrence rate RR ($N = 10\,000$). \mathcal{L} for surrogates are averaged over 100 realizations with error bars representing the standard deviation. (Online version in colour.)

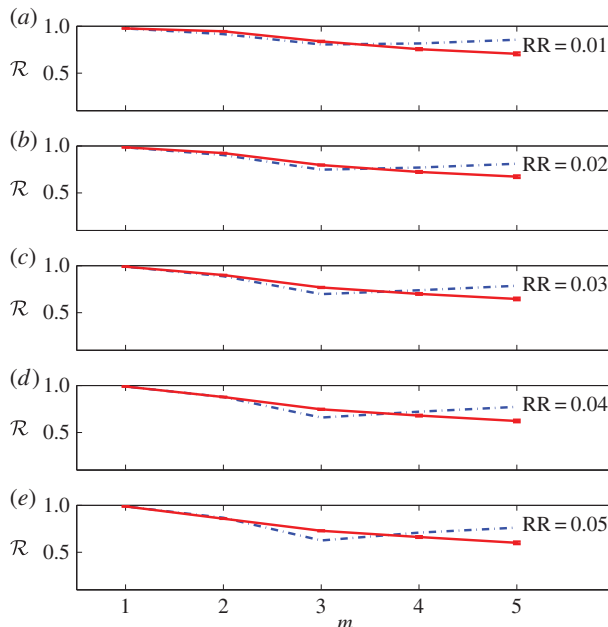


Figure 3. Assortativity \mathcal{R} of the ε -recurrence networks constructed from the x -component of Lorenz system (dashed blue lines) and corresponding iAAFT surrogates (solid red lines) for varying embedding dimension m and recurrence rate RR ($N = 10\,000$). \mathcal{R} for surrogates are averaged over 100 realizations with error bars representing the standard deviation. (Online version in colour.)

UPOs are the skeleton of chaotic dynamics, and there are infinitely many densely packed UPOs in such a system [60], whereas stochastic dynamics are not characterized by the presence of UPOs. Because D_T is essentially a measure of the global dimension of the system [39], presence of UPOs (especially low-periodic ones) should result in values of $D_T < m$ for increasing values of m , whereas in the case of stochastic dynamics, D_T should continue to increase with m . Our results reflect this behaviour and show how D_T can be used to distinguish between chaotic and stochastic dynamics. Note that at $m = 1$, D_T of both chaotic and stochastic dynamics is the same, i.e. ≈ 1 , and as m is increased, the difference in the D_T emerges between these two systems. This due to the fact that at $m = 1$, both the x -component of the Lorenz system and its corresponding iAAFT surrogate share the same invariant density [15,36]. Regarding the behaviour of \mathcal{L} , we can see from figure 2 that the ε -recurrence networks derived from iAAFT surrogates exhibit lower values of \mathcal{L} compared with that of the Lorenz system and this difference increases with m . These observations for \mathcal{L} are also expected as more shortcuts are introduced in the phase space (owing to homogeneous filling of the phase space) for the stochastic data leading to lower average number of hops between two vertices in phase space. Thus, \mathcal{L} for the stochastic dynamics decreases with increasing m , whereas \mathcal{L} for chaotic dynamics slightly increases with increasing m . Note that, in a chaotic system, there exist such shortcuts as well leading to lower values of \mathcal{L} compared with periodic systems, again owing to relatively more homogeneous filling of the phase space, for a comparable attractor diameter and threshold ε [37]. However, compared with stochastic dynamics, the \mathcal{L} of chaotic dynamics is still higher as evident from our results. Similar results were obtained for D_T and \mathcal{L} in the case of the chaotic Rössler system.

Figure 3 shows the behaviour of \mathcal{R} for the chaotic (Lorenz system) and stochastic dynamics (iAAFT surrogates). In the case of chaotic dynamics, \mathcal{R} remains around the same level for $m > 1$ and only shows a slight tendency to increase with m at high values of RR . For instance, $\mathcal{R} \approx 0.85$, 0.81 and 0.78 for $RR = 0.01$, 0.02 and 0.03, respectively, for all values of $m > 1$, whereas \mathcal{R} ranges between 0.74–0.76 and 0.71–0.75 for $RR = 0.04$ and 0.05, respectively, as m is increased from 2 to 5. Meanwhile, we observe that in the case of stochastic dynamics, \mathcal{R} decreases linearly with

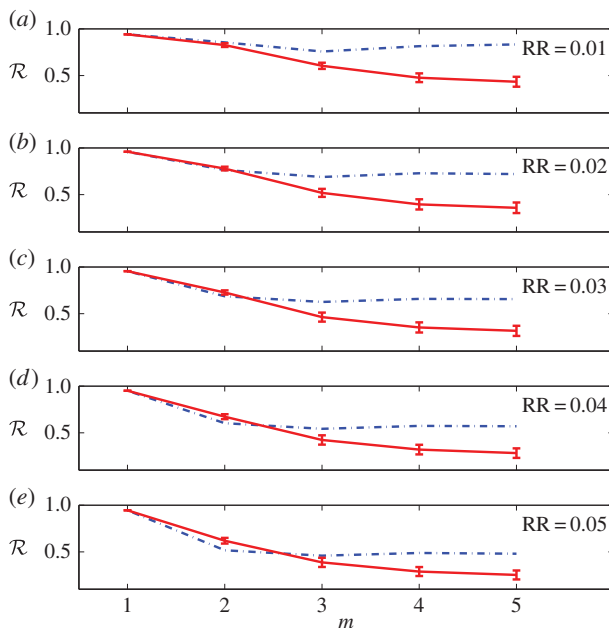


Figure 4. Assortativity \mathcal{R} of the ε -recurrence networks constructed from the x -component of the chaotic Rössler system (dashed blue lines) and corresponding iAAFT surrogates (solid red lines) for varying embedding dimension m and recurrence rate RR ($N = 10\,000$). \mathcal{R} for surrogates are averaged over 100 realizations with error bars representing the standard deviation. (Online version in colour.)

increasing m and for $m > 3$, the value of \mathcal{R} for stochastic dynamics drops below that of chaotic dynamics. As a network measure, \mathcal{R} measures the correlation of the degrees of the vertices on either ends of an edge. In a chaotic system, owing to the presence of UPOs, there exists a high-density clusters comprising vertices that roughly have the same degree and at an appropriately chosen threshold, this clustering property of the chaotic systems in the phase space is maintained, and the recurrence networks representing such systems should exhibit assortative mixing leading to high values of \mathcal{R} [61]. In our results, we consistently observe high values of \mathcal{R} (>0.7) for all values of RR and m for the Lorenz system, explaining the presence of densely packed UPOs, that form clusters. In the case of stochastic dynamics, the behaviour of \mathcal{R} is a bit ambiguous and difficult to interpret for $m \leq 3$. For higher values of m , we observe that the ε -recurrence networks representing the stochastic dynamics exhibits lower values of \mathcal{R} ($0.68 < \mathcal{R} < 0.52$) for $m = 5$ at various RR . Also, it can be seen that with the increase in RR , the value of \mathcal{R} drops. Following Donner *et al.* [14], this behaviour can be attributed to the larger coverage of the phase space owing to increasing RR leading to much stronger variation in phase space density, thus less similar degrees for neighbouring vertices. The behaviour of \mathcal{R} also seems to be system specific as in the case of the chaotic Rössler system (figure 4) it can be seen that at low values of RR (<0.04), \mathcal{R} can distinguish between chaotic and stochastic dynamics for $m > 2$. However, from our results, it is clear that \mathcal{R} can distinguish successfully between chaotic and stochastic dynamics at a sufficiently high embedding dimension, with ε -recurrence networks derived from chaotic dynamics exhibiting more assortative mixing compared with stochastic dynamics.

In the case of the hyper-chaotic Rössler system, it was observed that the difference between the (chaotic) deterministic and stochastic dynamics particularly improved as the number of data points was increased. We observed that, for low values of RR (<0.03) and m (≤ 3), there is an overlapping of D_T for hyper-chaos and stochastic processes (see electronic supplementary material, figure S1). Similar observations were made for the network measures \mathcal{L} and \mathcal{R} (electronic supplementary material, figures S2 and S3). From figure 5, it can be seen that \mathcal{L} distinguishes between hyper-chaotic and stochastic dynamics quite well for increasing m . As N is increased,

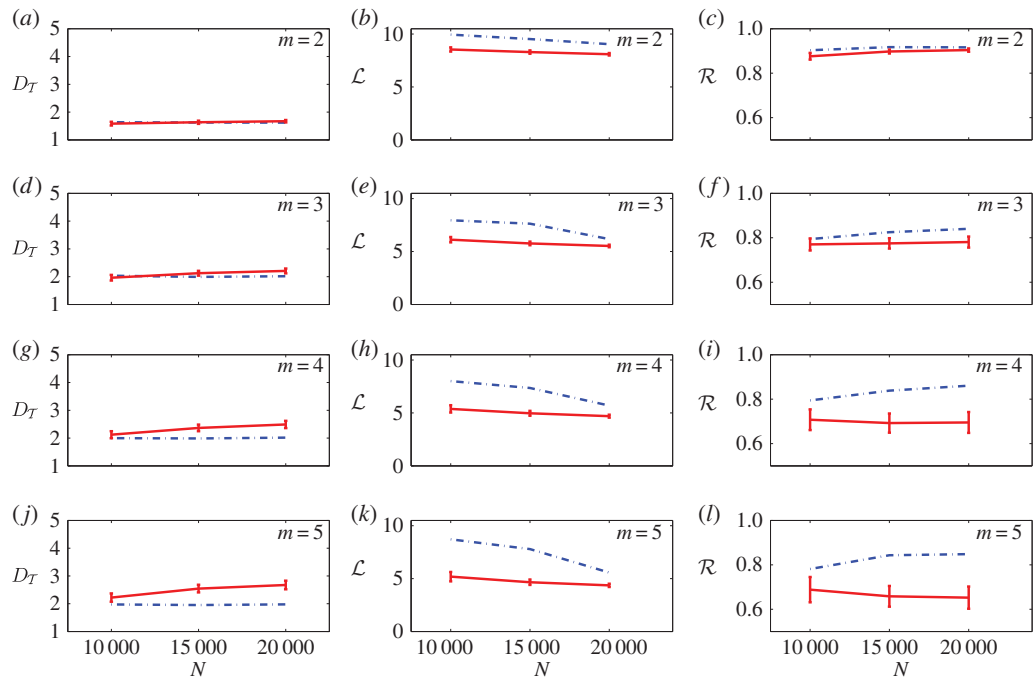


Figure 5. Transitivity dimension D_T (a), average path length \mathcal{L} (b) and assortativity \mathcal{R} (c) of the ε -recurrence networks constructed from the x -component of hyper-chaotic Rössler system (dashed blue lines) and corresponding iAAFT surrogates (solid red lines) for embedding dimension $m = 2$ and increasing data length N at recurrence rate RR = 0.02. The surrogates are averaged over 100 realizations with error bars representing the standard deviation. (d–f), (g–i) and (j–l) likewise in (a–c) but for $m = 3, 4$ and 5, respectively. (Online version in colour.)

\mathcal{L} for the hyper-chaotic system begins to decrease as the spread of the attractor increases in the phase space (hyper-chaos is better characterized geometrically with increasing data length) and this creates shortcuts between distant attractor points [60]. Also, in the case of network measures D_T and \mathcal{R} (figure 5), the distinction between hyper-chaotic and stochastic dynamics improved with increasing N and m . These results are expected as a higher number of data points leads to a better characterization of the underlying hyper-chaotic dynamics.

(c) Vertex-based network measures

The results for the vertex-based measures C_i , c_i , k_i and b_i for the Lorenz system, chaotic Rössler system, hyper-chaotic Rössler system and their corresponding iAAFT surrogates are presented and discussed in this section. In order to compare the distribution of the local measures for the (hyper)chaotic attractor and the corresponding iAAFT surrogate, we used the two-sample Kolmogorov-Smirnov (KS-2) test. The result from the KS-2 test for the vertex-based measures is shown in figure 6 for the Lorenz system. For the Lorenz system, it can be seen that the KS-statistic, which gives the maximum of the absolute difference between the cumulative distribution functions of the two samples (e.g. between the Lorenz attractor and the iAAFT surrogate), for the vertex-based measure C_i increases with the embedding dimension m for all values of the recurrence rate RR. For $m > 1$ and all values of RR, the null hypothesis that the two samples are consistent with the same underlying distribution was rejected (at 5% significance level) with the p -value being very close to 0. Similar observations were made in the case of c_i , b_i and k_i . We also repeated the KS-test for different realizations of the original data and its corresponding iAAFT surrogate and found similar results as in 6. Thus, the distributions of the vertex-based measures for the chaotic attractors were significantly different from their iAAFT

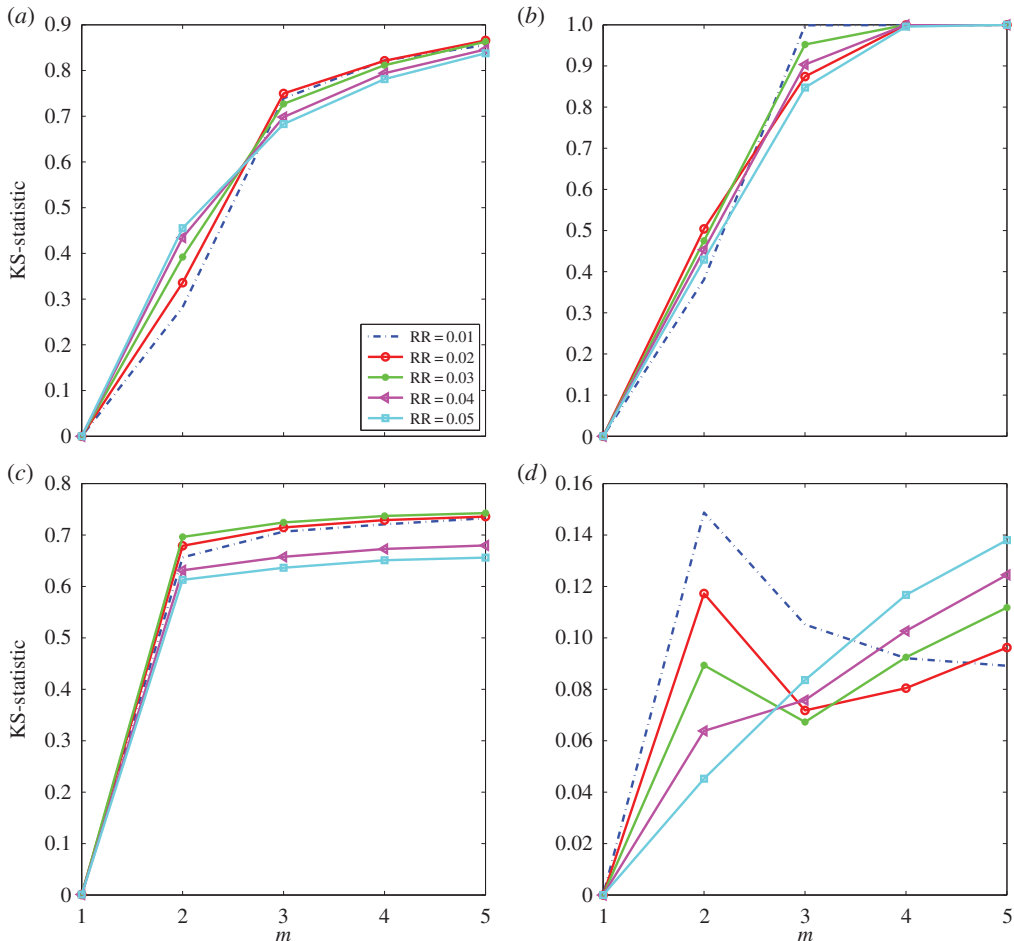


Figure 6. KS-statistic for (a) the local clustering coefficient C_i , (b) closeness centrality c_i , (c) betweenness centrality b_i and (d) degree centrality k_i for the Lorenz system ($N = 10\,000$) and the corresponding iAAFT surrogate for varying embedding dimension m and recurrence rate RR. (Online version in colour.)

surrogates for $m > 1$ and for all values of RR. An exemplary result from the KS-2 test for the chaotic Rössler attractor and the corresponding iAAFT surrogate is shown in figure S4 (electronic supplementary material). Additionally, electronic supplementary material, figures S8–S11 show the colour-coded representation of the vertex-based measures for the chaotic attractors (Lorenz and Rössler attractor) and their corresponding surrogates. It is evident from these figures that there exists clear difference in the spatial distribution of the vertex-based measures for chaotic and stochastic dynamics.

Figure 7 shows the relationship between b_i and C_i for the reconstructed chaotic attractors (Lorenz and Rössler) and their corresponding iAAFT surrogates. As a vertex-based measure, C_i reflects for a given vertex, the density of the links between its neighbours. In the context of an ε -recurrence network, the measure C_i is related to the geometric alignment of the vertices in the phase space [14]. For instance, the vertices along the stable manifold of a UPO are characterized by high values of C_i and because UPOs are the backbone of chaotic attractors, the measure C_i is particularly important for the geometric characterization of chaos. Furthermore, the vertices belonging to a sparse region (that separate high-density clusters like the vertices belonging to the stable manifold of a UPO) in the phase space acquire high values of b_i as they act as transfer vertices or hubs between two high-density clusters on the either side of the sparse region [14,62]. Also, these vertices exhibit low values of C_i as they belong to sparse region in phase space and

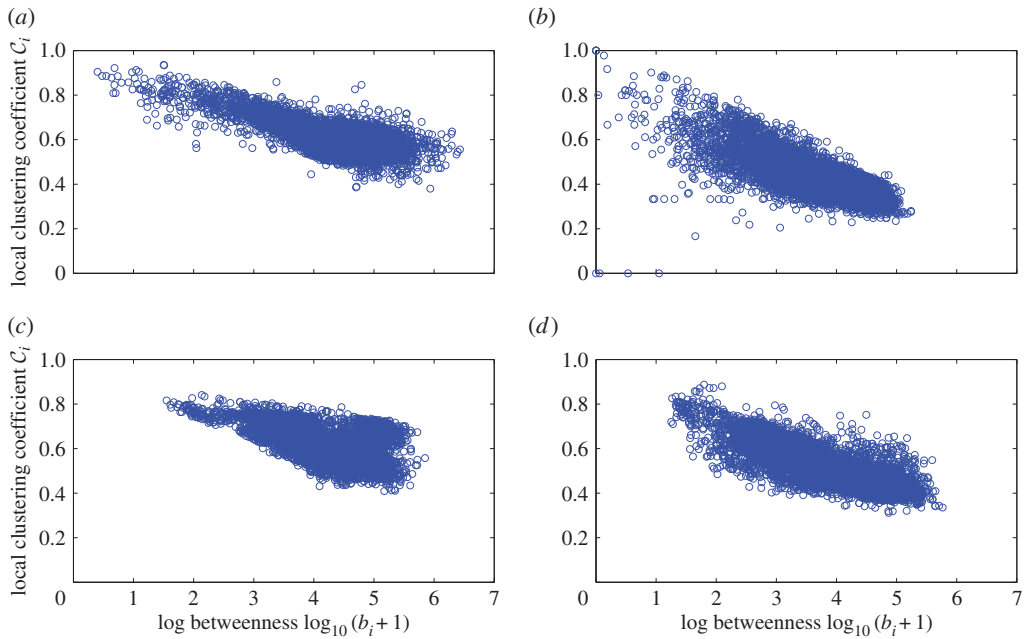


Figure 7. Variation of log betweenness centrality $\log_{10}(b_i + 1)$ with the local clustering coefficient C_i for the Lorenz attractor (a) and the corresponding iAAFT surrogate (b). (c)–(d) same as (a)–(b) but for the chaotic Rössler attractor and the corresponding iAAFT surrogate. The parameters for the exemplary plot are, embedding dimension $m = 5$ and RR = 0.02. (Online version in colour.)

lack clustering properties compared with the vertices within the high-density clusters. Thus, the vertices belonging to the high-density cluster in the phase space must exhibit high values of C_i and low values of b_i . These points are clearly reflected in figure 7a,c where it can be seen that for the chaotic dynamics (Lorenz and Rössler system), more vertices with low values of b_i (for convenience, we have plotted $\log_{10}(b_i + 1)$) exhibit high values of C_i compared with the stochastic dynamics (figure 7b,d). The obvious reason for this difference is that the stochastic dynamics are not characterized by the presence of UPOs and, hence, there are no high-density clusters and consequently less number of vertices acting as hubs between high-density clusters to acquire high values of b_i . Also, we can see the expected trend of vertices with high values of b_i exhibiting low values of C_i from figure 7. The difference between chaotic and stochastic dynamics is also evident here, as the value of C_i acquired by vertices (displaying high values of b_i) belonging to ε -recurrence networks constructed from iAAFT surrogates are much lower than their chaotic counterparts. Xiang *et al.* [62] studied the relationship between C_i and b_i with adaptive nearest neighbour recurrence networks for the chaotic Rössler system and found that vertices with low b_i display high C_i , an observation our results support as shown in figure 7a,c support.

The ε -recurrence networks constructed from chaotic systems contain more vertices that display high values of b_i (>3000 vertices with approximately 10^4 shortest paths) and C_i (>3000 vertices with $C_i \approx 0.6$) compared with the ε -recurrence networks constructed from the stochastic dynamics in the case of the Lorenz attractor and the corresponding iAAFT surrogate (electronic supplementary material, figure S12). Thus, the presence of UPOs in the chaotic dynamics is captured geometrically by the local vertex-based measures such as C_i and b_i . However, it has to be noted here that, in the case of chaotic dynamics, although vertices with low betweenness exhibit very high C_i , there exists broad range of values for betweenness centrality for vertices displaying high C_i (≈ 0.6) and as noted in reference [63], b_i alone cannot confirm the presence of UPOs.

Next, we looked at the relationship between b_i and k_i in chaotic and stochastic systems. The vertex measure k_i is related to the local phase space density while the measure b_i depends on

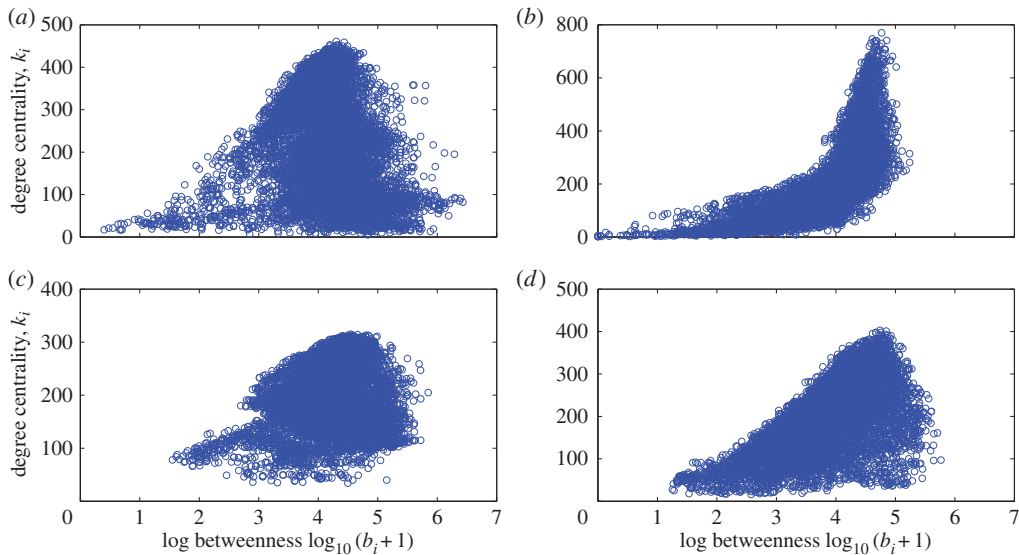


Figure 8. Variation of log betweenness centrality $\log(b_i + 1)$ with the degree k_i for the Lorenz attractor (a) and the corresponding iAAFT surrogate (b). (c, d) same as (a, b) but for Rössler attractor and the corresponding iAAFT surrogate. The parameters for the exemplary plot are, embedding dimension $m = 5$ and RR = 0.02. (Online version in colour.)

the relative number of shortest paths that pass through i . It can be seen from figure 8 that in the case of chaotic dynamics (Lorenz and Rössler), the vertices that exhibit low value for b_i ($< 10^3$ shortest paths) also exhibit low value for k_i . These are specifically the vertices in the vicinity of the outer boundaries of the attractors. This effect is enhanced in the case of Lorenz attractor, where we observe more vertices exhibiting low values for b_i and k_i simultaneously compared with the Rössler attractor as in the case of the Lorenz system the outer parts of the attractor that are not involved in the shortest paths, exhibit low phase space density [63]. In the case of stochastic dynamics, we see this trend as well where vertices with low b_i also acquire low k_i . However, owing to the presence of UPOs, an interesting region is observed in the b_i versus k_i graph in the case of chaotic dynamics which is missing in stochastic dynamics. The vertices that are in the vicinity of UPOs acquire somewhat low values for b_i owing to the accumulation of states leading to increased shortest paths [63]. But, these vertices in the vicinity of the UPOs, acquire relatively high values for k_i owing to the very same reason of accumulation of states. This fact is clearly reflected in figure 8a,c, where vertices with $10^4 \leq b_i \leq 10^6$ acquire $200 < k_i < 300$. This middle region of the graph is completely missing in the case of the corresponding iAAFT surrogates (figure 8b,d).

Furthermore, in the case of chaotic dynamics, it can be seen that some of the vertices that acquire high values of b_i ($> 10^4$) have a broad range of k_i (50–400) as these vertices reside in the sparse region of phase space and mostly have vertices in the high-density clusters as their neighbours. In the case of the stochastic dynamics, we can see that the range for b_i for a given value of k_i is much narrower compared with chaotic dynamics. The reason for this can be that in the case of stochastic dynamics, the sparse regions between two high-density clusters do not exist as in the case of chaotic dynamics, but rather the space is uniformly filled with vertices. This increases the total number of shortcuts between pairs of vertices thus reducing the b_i for a vertex i through which some of the shortcuts pass. Furthermore, few of the vertices (which would otherwise been a part of sparse region) tend to have more neighbours owing to homogeneous filling of the phase space increasing the value of k_i (up to 800). However, most of the vertices in the case of stochastic dynamics tend to have low degree that display b_i between 10^3 and 10^5 .

The distribution of c_i in the case of chaotic dynamics (Lorenz attractor) is clearly different compared with the stochastic dynamics (see electronic supplementary material, figure S13). Specifically, in the case of chaotic dynamics, most of the vertices (≈ 6500) acquire c_i between

0.1 and 0.11, these vertices particularly belong to the centre of gravity of the chaotic attractors [14]. In the case of stochastic dynamics, owing to the existence of many shortcuts, a relatively broad range of c_i (between 0.23 and 0.3) is acquired by the vertices. Because c_i used in this work follows the definition in reference [43], where c_i is essentially defined as the inverse of average shortest path length of a vertex to all other vertices in a network (see equation (2.5)), the vertices of ε -recurrence networks constructed from iAAFT surrogates tend to have larger values owing to increased shortcuts, compared with the networks representing chaotic dynamics. The distribution of k_i has multiple peaks owing to many UPOs embedded in chaotic attractors [61] (e.g. at 100, 200 and 400 in electronic supplementary material, figure S13), whereas the distribution of k_i in the case of stochastic dynamics is skewed and most of the vertices have a low degree of around 150–200.

In the case of the hyper-chaotic Rössler system, the value of the KS-statistic increased as the data length was increased (electronic supplementary material, figures S5–S7), specifically in the case of the vertex-based measures C_i and b_i . Looking at the distributions of b_i and C_i for the hyper-chaotic Rössler attractor and the corresponding surrogate at $N = 10\,000$ and $20\,000$ (electronic supplementary material, figures S14 and S16), it is clear that the nodes acquiring high values of b_i and C_i in ε -recurrence networks constructed from the hyper-chaotic Rössler system increases compared with the networks constructed from the corresponding iAAFT surrogates as data length is increased. Also, looking at the distributions of c_i and k_i (electronic supplementary material, figures S15 and S17 for $N = 10\,000$ and $20\,000$, respectively), we again observe that vertices of the ε -recurrence networks representing hyper-chaotic dynamics tend to acquire lower values of c_i compared with their stochastic counterparts for the same reason as outlined above for the chaotic case. On similar lines, the distribution of k_i again shows multiple peaks in the case of hyper-chaotic dynamics, which is missing in the case of its stochastic counterpart.

(d) Effect of noise

Figure 9 shows the impact of noise on the global measures D_T , \mathcal{L} and \mathcal{R} . In the case of D_T , it can be seen that at 0% noise (i.e. noise-free case) the value of D_T is less than 2 for increasing dimension for various RR. More specifically, as RR is increased, the value of D_T drops. For instance, at RR = 0.05, D_T is around 1.7 to 1.8, whereas at RR = 0.01, D_T is around 1.4 to 1.5, and these values remain approximately at the same level for $m > 2$. In the following, we will only discuss results pertaining to $m > 2$, because $m = 3$ is the minimum dimension needed to unfold the dynamics of the Lorenz system. As the level of noise is increased, the value of D_T increases above 2 at noise level of 10% for RR = 0.01. As the RR is further increased to 0.03, the value of D_T remains under 2 at 10% noise level. On further increasing the RR to 0.05, even at the noise level of 20%, we can observe that $D_T < 2$ for $m > 3$.

At noise levels greater than 20%, irrespective of RR, the value of D_T becomes greater than 2 and continues to increase with noise. For example, at the noise level of 40%, $D_T = 2.38$ at RR = 0.05 and $m = 3$. This is due to the homogeneous filling of the phase space owing to the addition of the noise which makes the dynamics more stochastic, thus leading to an increase in the fractal dimension. In other words, as noise level increases, the local microscopic fine structure of the chaotic attractors, namely the densely packed UPOs, is destroyed. Because T essentially measures the clustering property, the distortion of the clustering property owing to the presence of UPOs results in lower values for T (equivalently a higher value for D_T) for noise levels greater than 20%. Regarding the behaviour of \mathcal{L} under noise, it can be seen from figure 9 that as noise increases, \mathcal{L} expectedly decreases, because more shortcuts are introduced with increasing noise levels in phase space leading to shorter paths. We can observe a drop of about 40–50% in the value of \mathcal{L} at noise level of 40% for $m > 2$. Also, the drop is sharper at low values of RR. Previously, we have shown that the global clustering coefficient (different from T but still related to the triangles in a network) and \mathcal{L} cannot distinguish between noisy periodic dynamics and noise-free chaotic dynamics at noise level greater than 20% and the influence of noise on the global clustering coefficient can be minimized by increasing the RR [28]. By increasing the RR and thus the ε , larger scales are captured owing to which the impact of noise amplitudes on measures like T

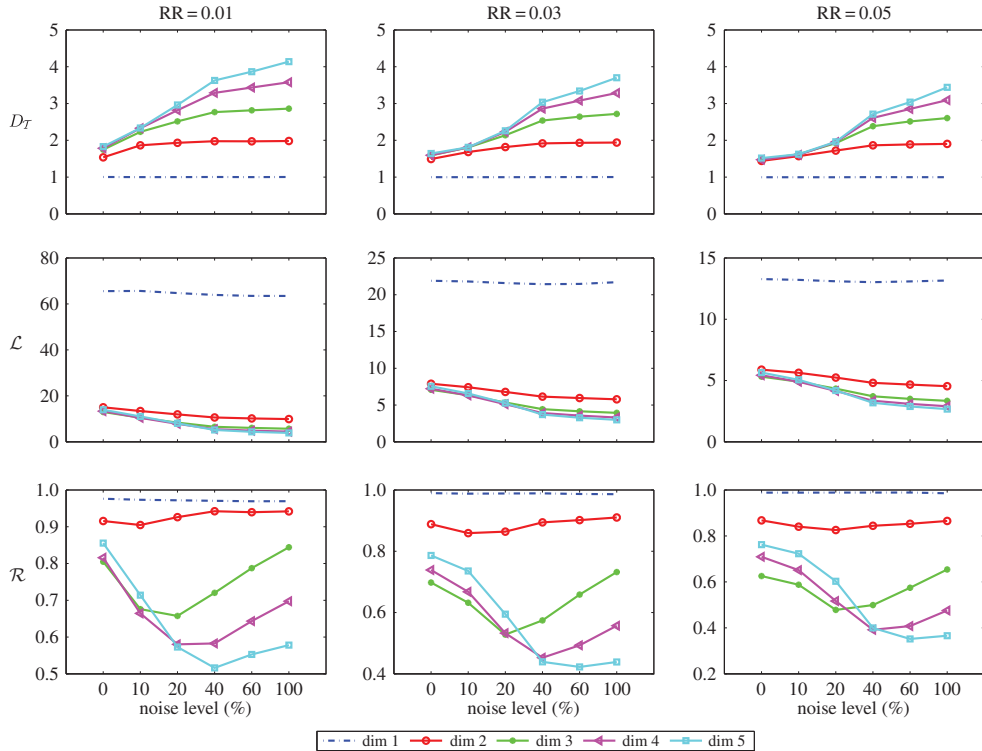


Figure 9. Effect of noise on the global measures for the Lorenz system for varying noise level and recurrence rate. (Online version in colour.)

and the global clustering coefficient is reduced. With respect to the behaviour of \mathcal{R} under noise, it can be seen from figure 9 that for $m > 2$, the value of \mathcal{R} decreases as noise levels increase, however, this behaviour is modulated by the choice of RR. For low values of RR such as 0.01, it can be seen that \mathcal{R} decreases up to noise level of 20%. Interestingly, as the noise level is increased beyond 20%, \mathcal{R} starts to increase. However, the increase in \mathcal{R} is further constrained by the embedding dimension m and we observe that very high noise levels ($>20\%$), $\mathcal{R}_{m=5} < \mathcal{R}_{m=4} < \mathcal{R}_{m=3}$. We see this trend at other values of RR as well, however, as RR increases, at $m = 5$, \mathcal{R} continues to decrease with increase in noise levels up to 60%. Thus, at $m = 5$, \mathcal{R} shows expected behaviour with the addition of noise, where \mathcal{R} decreases with the addition of noise and drops to a value less than 0.4 at 60% noise. As mentioned previously (see §3b), sufficiently higher m ($m = 5$ in the case of Lorenz attractor) is required for a reliable structural characterization of chaotic attractors with \mathcal{R} .

Next, we investigated the influence of noise on the vertex-based measures C_i , b_i , c_i and k_i . In the case of C_i and b_i , as noise is increased the number of vertices acquiring high values for both these measures decrease compared with the noise-free case as shown in the first two columns of figure 10 where it is evident that the distributions shift left with increasing noise. In the case of b_i , in the noise-free case, there are ≈ 3000 vertices with approximately 10^4 shortest paths and this drops to approximately 2000 at 40% noise. In the case of C_i , there are ≈ 3000 vertices with $C_i \approx 0.6$ and this drops to ≈ 500 vertices at 40% noise. The reason for this is again related to the distortion of the clustering structure as noise is added to chaotic dynamics, which impacts both these measures. In the case of c_i , we see that the number of vertices acquiring high values of c_i increase with the addition of noise (third column from left, figure 10). As noise is added, there are more shortcuts in the phase space owing to homogeneous filling which reduces the length of shortest paths, which is inversely related to c_i (equation (2.5)). In the case of k_i , where one can observe multiple peaks in noise-free case (owing to many UPOs) [64], addition of noise makes the distribution more skewed (and long tailed) and the number of vertices with low degree increases

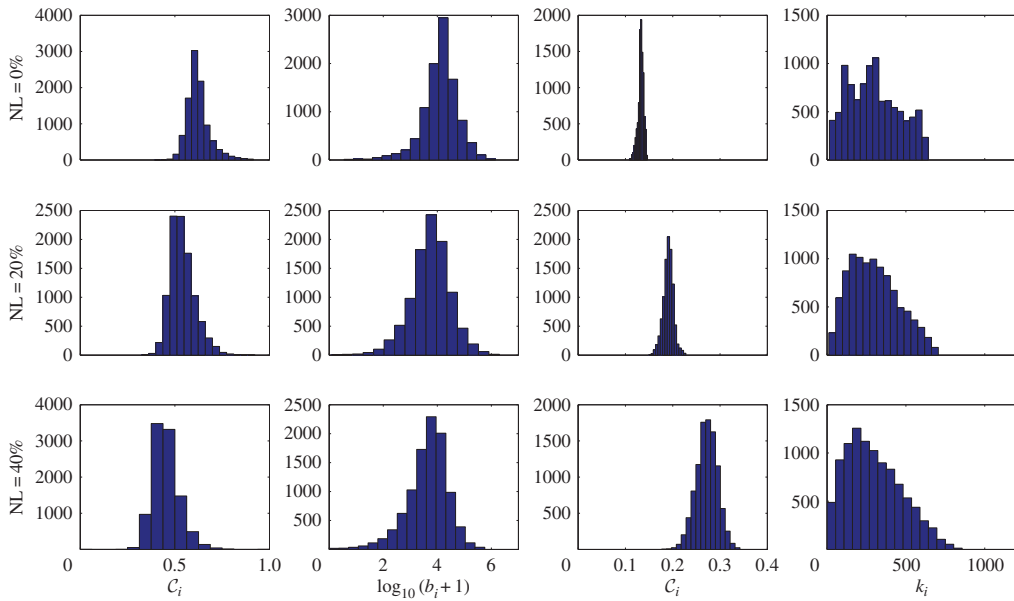


Figure 10. Impact of noise on vertex-based measures for the Lorenz system. Parameters for the exemplary plot are RR = 0.03 and $m = 5$. (Online version in colour.)

as the noise is increased (last column, figure 10). Figure 11 shows the impact of noise on the b_i versus C_i for various RR. From figure 11a–c, it can be seen that with the addition of noise, at RR = 0.01, the number of vertices exhibiting low C_i and b_i increases. As the RR is increased to 0.05 (figure 11g–i), we can see that vertices having low b_i tend to acquire high values of C_i , a behaviour observed in noise-free chaotic dynamics. Thus, increasing RR can minimize the influence of noise on the clustering property ε -recurrence networks representing chaotic dynamics in phase space. Similar observations were made for Rössler and hyper-chaotic Rössler system.

(i) Effect of data length and comparison with complexity–entropy method

Table 1 shows the number of rejections (out of 100 realizations) of null hypothesis H_0 of a linear, Gaussian-correlated noise undergoing a nonlinear static transformation [40], for various noise levels and data lengths using global network measure \mathcal{T} at RR = 0.05 for the Lorenz system. Results using the C–E causality plane method described in references [3,65] to distinguish between chaos and noise is also shown for comparison, where we set $m = 3$ and $\tau = 3$. The C–E method uses two quantifiers—the Shannon entropy [66] and the MPR statistical complexity measure proposed by Lamberti *et al.* [67]. Before estimating quantifiers based on information theory like entropy or the statistical complexity measure, a probability distribution associated with the time series must be provided. As described in reference [3], we use Bandt–Pompe methodology [68] to estimate the probability distribution P using the details of attractor reconstruction procedure (Taken’s theorem) and causal information is incorporated in the construction process yielding $P \in \Omega$, where Ω is the probability space. The entropy estimates the uncertainty associated with the processes described by P , whereas the MPR complexity measure is capable of distinguishing different degrees of periodicity and chaos. The details of the C–E method and computation of the probability distribution using Bandt–Pompe methodology is explained in detail elsewhere [3,65]. We provide freely downloadable MATLAB code based on [3,65] to compute the C–E causality plane.

Two exemplary plots (see electronic supplementary material, figures S18 and S19) are shown using the C–E method to distinguish between chaotic time series and the corresponding iAAFT surrogates under varying noise levels for data length $N = 200$ and 1000, respectively. It is evident

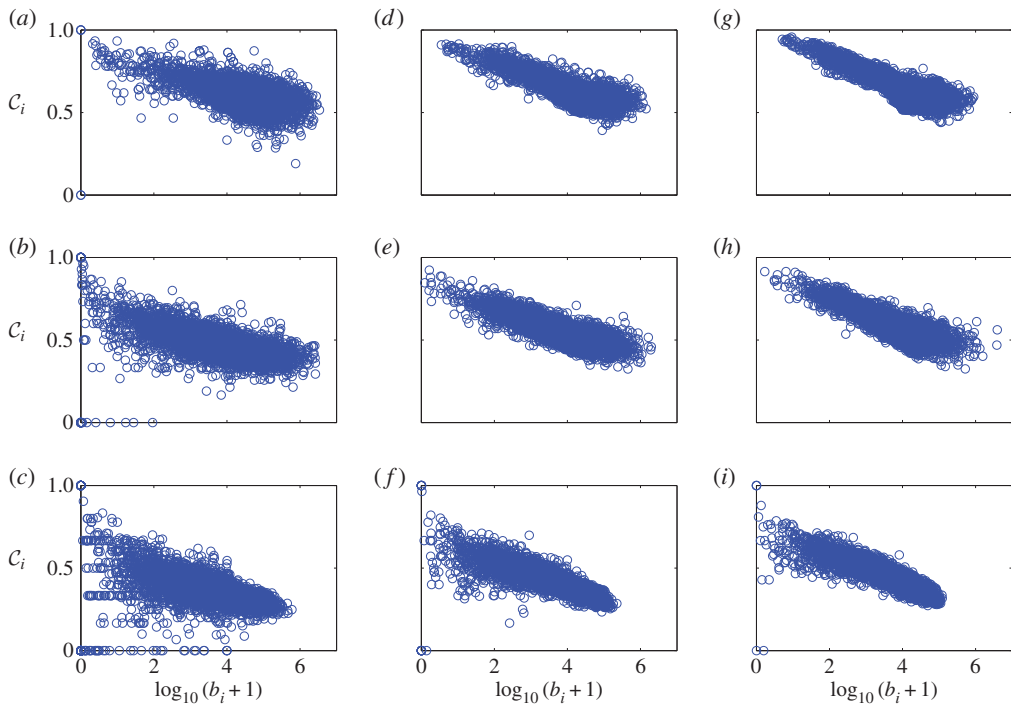


Figure 11. (a–c) Variation of log betweenness centrality $\log(b_i + 1)$ with the local clustering coefficient C_i for the Lorenz attractor for $RR = 0.01$ at noise level (a) 0%, (b) 20% and (c) 60%. Panels (d–f) and (g–i) same as (a–c) but for $RR = 0.03$ and $RR = 0.05$, respectively. (Online version in colour.)

from these figures that under noise-free condition, the position of the chaotic signal maps on to a different position on the C-E plane compared with the surrogates (stochastic signal). The complexity of the chaotic signal is higher than that of the surrogates, whereas the entropy of the chaotic signal is lower than that of the surrogates. As the chaotic signal is corrupted with noise, we can see that at short data length (see electronic supplementary material, figure S18), at noise levels greater than 10%, the location of the noisy chaotic signal on the C-E plane falls within that of the 99 surrogates and is no longer distinct. When the data length is increased to $N = 1000$ (see electronic supplementary material, figure S19), we can see that a clear distinction between noisy chaotic signal and its corresponding iAAFT surrogates can be made up to a noise level of 40%.

Without making any assumption about the distribution of the test statistic, we use the non-parametric approach (based on rank ordering) to test the null hypothesis H_0 [42] (We obtained qualitatively similar results when the parametric approach using the mean and standard deviation of surrogates was used). Because a chaotic time series should produce high values of complexity compared with a stochastic signal and a stochastic signal displays higher entropy values compared with deterministic (chaotic) signal [3], the null hypothesis of a linear, Gaussian, stochastic process can be rejected if the complexity of the signal is greater than the maximum of the surrogates and the entropy of the signal is lesser than the minimum of the surrogates. In the case of ε -recurrence network measures such as T , L and R , the null hypothesis H_0 is rejected if the ε -recurrence network measure of the signal under test is greater than the maximum of the ε -recurrence network measures of the surrogates [28,69]. Because we are using 99 surrogates, the probability with which a false rejection will occur is $\frac{1}{100}$ (i.e. $\alpha = 0.01$). We can see that at $N = 200$, compared with the C-E method, T gives comparatively higher rejections of H_0 , even when the noise level is 40% (table 1). Even at 60% noise level, T gives a significant number of rejections (=16), whereas the C-E method fails to reject H_0 for all the 100 realizations. Thus, the recurrence network measure T is still able to reject H_0 with high confidence for short time series

noise levels as high as 60%. Qualitatively similar observations were made for the Rössler system (results not shown here).

We also observed that as the noise level is increased, the topology of the ε -recurrence network changes and it tends to fill the phase space (see electronic supplementary material, figures S20–S22). However, the topology of the ε -recurrence network, which is reflective of the topology of the embedded attractor (Lorenz attractor in this case) is not completely destroyed even at short data length of $N = 200$ and considerably high noise levels up to 40%. As noise level is increased (60% and 100%), we see that the topology of the ε -recurrence network does not resemble the shape of the Lorenz attractor and the network tends to fill the phase space.

Electronic supplementary material, Figures S23 and S24 show the colour-coded representation of the local clustering coefficient and log betweenness centrality, respectively, for the ε -recurrence networks under increasing levels of noise for the Lorenz system. Under noise-free condition, most of the vertices have high values for C_i , but as the level of noise increases, many vertices start displaying low values for C_i and the topology of the ε -recurrence network changes as well owing to the addition of noise. As mentioned earlier (also see figure 10), owing to the addition of noise, the clustering structure associated with ε -recurrence networks derived from chaotic systems gets distorted leading to lower values of C_i for many vertices. Similarly, as the noise level is increased, a higher number of vertices acquire lower values of log betweenness centrality (figure 10). Electronic supplementary material, figure S25 shows the colour-coded representation of the local recurrence rate, which is proportional to degree centrality, for the Lorenz attractor under increasing levels of noise. It is clear from the figure that as the noise level increases, the local recurrence rate for most of the vertices decreases and at very high noise levels most of the vertices tend to have similar values for the local recurrence rate. This effect can also be seen from figure 10 where the shape of the degree distribution changes from having multiple peaks (owing to the presence of UPOs) under a noise-free case to approaching a Poisson distribution with the addition of noise.

4. Experimental electroencephalography data with seizures

(a) Electroencephalography data

Here, we demonstrate the ability of ε -network measures to capture dynamical transitions in noisy biological signals such as EEG data using rather short window sizes. Epilepsy affects nearly 1% of the world's population and epileptic seizures arise owing to unpredictable and irregular interruptions in the neuronal activity [70]. The EEG data used in this work were originally published by Quiroga *et al.* [71] and are available for free download at <https://vis.caltech.edu/~rodri/data.htm>. Basically, the data comprise tonic-clonic seizures of two subjects recorded using scalp EEG with right central electrode (channel C4 according to 10–20 system [72]). The EEG data have been filtered between 1 and 50 Hz and sampled at 102.4 Hz. Figure 12a shows 3 min of EEG data from one of the two patients. The beginning of the seizure is marked with a solid red line (approx. at 80 s). The seizure discharge lasts for about 8 s, and the clonic phase begins at 123 s (marked with dashed red line) [71]. The seizure ends approximately around 155 s (marked with solid black line). Also at around 140 s (not shown in the figure), the clonic discharge begins to separate [71].

(b) Moving window ε -recurrence network analysis

We used moving window ε -recurrence network analysis to compute global measures such as D_T , \mathcal{L} and \mathcal{R} for each window. We divided the time series into 5 (≈ 500 samples) and 10 s window (≈ 1000 samples) with 90% overlap. In order to get the temporal profile of global network measures, we assigned the global measure to the mid-point of each window. Based on the first local minimum of the auto mutual information function, we set $\tau = 18$. The embedding dimension

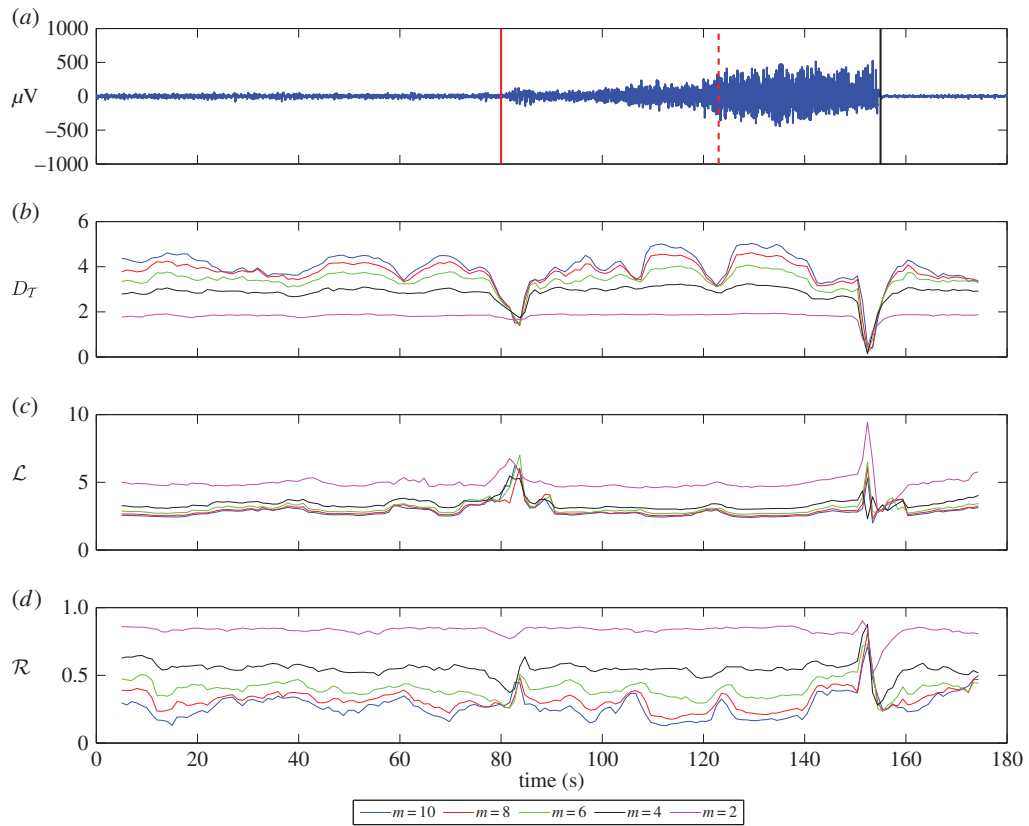


Figure 12. Moving window ε -recurrence network analysis of epileptic EEG data show D_T , \mathcal{L} and \mathcal{R} before, during and after the seizure. (a) EEG data from channel C4 of patient 1 with the clinical onset of seizure marked with solid red line. The dashed red line represents beginning of the clonic phase and the solid black line represents that end of seizure. (b–d) Temporal profile of the global measures (for $m = 2, 4, 6, 8, 10$) using a moving window of 10 s (≈ 1000 samples) with 90% overlap. (Online version in colour.)

m was varied from 2 to 8, and the recurrence rate RR was set to 0.05. Figure 12b–d shows the result of ε -recurrence network analysis for the EEG data with 10 s window.

- Transitivity dimension:* it can be seen that D_T increases with embedding dimension m until about 80 s before the seizure. Beyond 80 s, D_T starts to drop for $m \geq 4$. For $m = 2$, we do not observe much variation in D_T . This result for D_T clearly indicates that just before the beginning of the seizure at 80 s, the global dimension as measured by D_T begins to drop even if the m is increased up to 10, a characteristic associated with a (low-dimensional) deterministic system. This behaviour is seen again at around 120 s when the clonic phase of the seizure begins. Towards the end of the seizure, D_T again drops and remains at the same level for increasing values of m . The period after the seizure is characterized again by values of D_T that increase with embedding dimension m .
- Average path length:* regarding the behaviour of \mathcal{L} , one can observe that starting around 70 s, there is a ramping up of \mathcal{L} for increasing m ($m \geq 4$) and \mathcal{L} peaks at around 84 s, which coincides with the time of the local minima for D_T for the seizure period. \mathcal{L} then starts to decrease and again begins to increase at around 140 s and peaking at around 150 s. In the post-seizure period, we can see that as the value of m increases the value of \mathcal{L} decreases (as observed in the pre-seizure period). The temporal profile of \mathcal{L} is more clearly depicted for $m = 8$ in figure 13c.

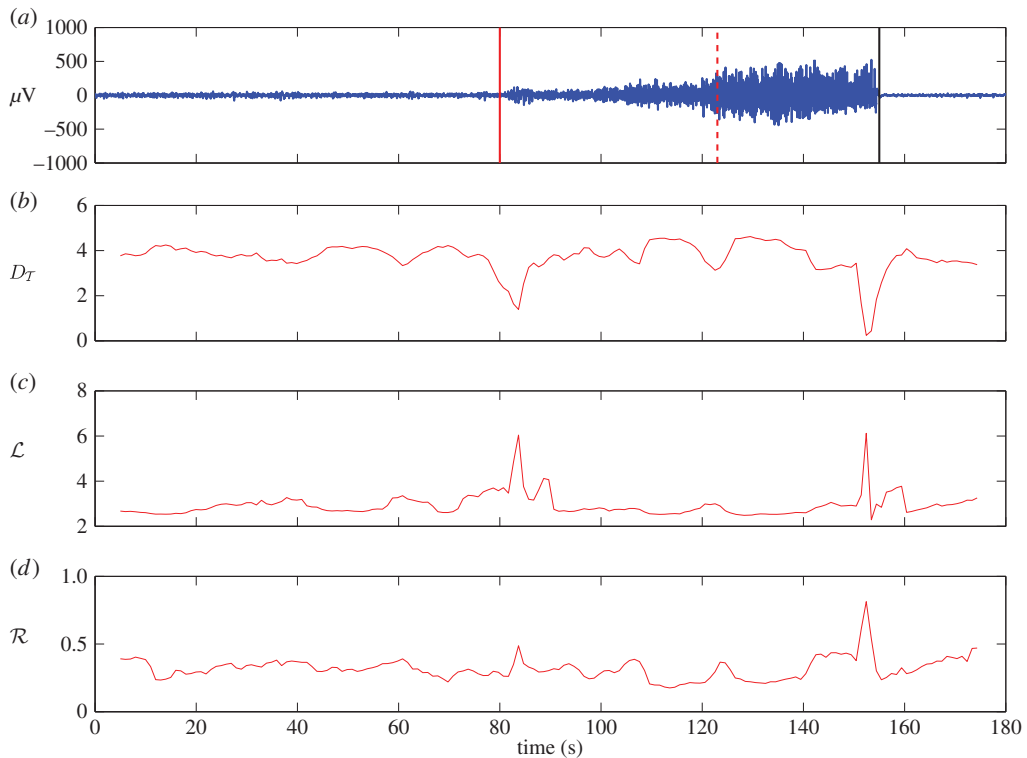


Figure 13. Moving window ε -recurrence network analysis of epileptic EEG data showing D_T , \mathcal{L} and \mathcal{R} before, during and after the seizure. (a) EEG data from channel C4 of patient 1 with the clinical onset of seizure marked with solid red line. The dashed red line represents beginning of the clonic phase and the solid black line represents that end of seizure. (b–d) Temporal profile of the global measures (for $m = 8$) using a moving window of 10 s (≈ 1000 samples) with 90% overlap. (Online version in colour.)

(iii) *Assortativity:* the behaviour of \mathcal{R} becomes clear only for $m \geq 6$, where \mathcal{R} begins to increase from 70 s reaching its local maxima at around 84 s, which coincides with the local minima for D_T for that period. It then begins to drop and again tends to increase at around 140 s and peaks at around 150 s. Around the seizure period, for $m \geq 6$, irrespective of the value of m , the value of \mathcal{R} remains approximately around the same value. (Also see figure 13d).

We make the following crucial observations based on the application of ε -recurrence network analysis to the EEG data.

- (i) It is clear from the above results that the measures D_T , \mathcal{R} and \mathcal{L} are not entirely independent and they track dynamical transitions in a related fashion.
- (ii) These three measures, as applied to the EEG data at hand, start showing signs of change well before the clinical identification of seizure (compare the clinical onset of seizure in figure 13a with the point when the global network measures start increasing (or decreasing in the case of D_T) in figure 13b–d). This feature represents the possibility of using these measures to predict the seizure in advance. However, note that, in the dataset used, the clinical onset of the seizure occurs just 80 s into the data. Having a longer segment of data before the seizure onset could also reveal interesting shifts in dynamics much prior to the onset of the seizure. Recent studies have shown that it is possible to detect interesting changes in EEG tens of minutes before the actual seizure occurrence [73,74]. However, most of these measures require long window sizes, of the order of 10 min, which is related to our next observation.

- (iii) The global network measures are able to capture the rapidly changing dynamics using short windows of 5 (512) and 10 s (1024) samples, which is one of the key advantages of ε -RNA compared with other methods. It is well known that the epileptic seizures exhibit high nonlinearity compared with the normal background EEG activity [75] as demonstrated in references [76,77]. Previously, we have also demonstrated that ε -recurrence networks derived from EEG recorded during the seizures display high values for the global clustering coefficient and average path length compared with networks derived from normal and interictal (EEG between seizures) activity, thus capturing the increase in nonlinearity and the associated structural complexity of the data [28]. However, the results in reference [28] were obtained with EEG data of length 20 s (2560 samples) which is still long compared with the window size of 5 (512 samples) and 10 s (1024 samples) chosen in this study
- (iv) In the case of patient 1, the clonic phase begins around 123 s, and we observe that all the three global measures, display shift in their dynamics around this time point (figure 13b-d). Also, we observed an increase in D_T and decrease in \mathcal{L} and \mathcal{R} , before these measures stabilize in the post-seizure period, which can be considered as a surrogate marker. This shift in dynamics is also consistent with the analysis in reference [71] using Gabor transform and could represent decrement in neural firing along with increase in inhibitory mechanisms, that could be responsible for seizure termination [71]. However, further research is needed to relate the variation of global ε -recurrence network measures towards the transition to postictal activity.
- (v) The results based on these global measures suggest that the EEG signals before and after the seizure are more consistent with stochastic dynamics and during the seizure, the dynamics is more deterministic.

Qualitatively, similar results were found for patient 2 (electronic supplementary material, figure S26) and with window size of 5 s (electronic supplementary material, figure S27). These are novel and interesting results for the application of ε -recurrence network analysis to epileptic EEG data. However, these observations are based on the dataset from only two patients and would need an extensive further study involving data from a large number of patients and different types of epilepsies to draw a more substantiated conclusion. Also, we have considered data from only one channel. Recent studies have shown evidence of seizure onset within networks of brain regions known as epileptic networks [78,79]. Hence, an approach taking into account functionally connected brain regions [80] is more advantageous. The possibility of using cross and joint recurrence network measures [58,81] to derive functional networks using multivariate epileptic EEG data will be considered in the future.

5. Conclusion

In summary, we have shown that ε -network measures, both global and vertex-based, can be used to distinguish between (hyper-)chaotic and stochastic dynamics. We also demonstrated the effect of noise on these network measures. As a real-world application, we have shown that moving window ε -recurrence network analysis can detect dynamical shifts in epileptic EEG data.

We have shown that measures such as transitivity \mathcal{T} (or the related global dimension measure, the transitivity dimension D_T), local clustering coefficient \mathcal{C}_i , degree centrality k_i and betweenness centrality b_i are particularly sensitive to the presence of UPOs, which are the geometric backbone of the chaotic attractors. Additionally, other global measures such as average path length \mathcal{L} and assortativity \mathcal{R} were also able to distinguish between (hyper-)chaotic and stochastic dynamics. With assortativity \mathcal{R} , we particularly observed that the difference between chaotic and stochastic dynamics increased with embedding dimension and generally a large embedding dimension (e.g. $m = 5$ in the case of Lorenz system) is required for successful characterization of chaos. The vertex-based measure closeness centrality c_i is also sensitive to the geometry of chaos leading to small values for chaotic dynamics compared with stochastic dynamics. For the first time, to the best

of knowledge, we have demonstrated that the topological statistics derived from ε -recurrence networks can distinguish between chaotic and stochastic dynamics. In the case of hyper-chaotic dynamics, we further find that the distinction between chaotic and stochastic dynamics increases with data length. We have also shown in this study that, addition of noise impacts both global and vertex-based measures. Influence of noise levels on the clustering property of the ε -recurrence networks and the presence of unstable periodic orbits was evident with the increase in transitivity dimension D_T , decrease in number of vertices with high values for local clustering coefficient C_i and betweenness centrality b_i and disappearance of peaks (which is related to the UPOs) in the distribution of degree centrality k_i . The influence of noise on these measures can be minimized to some extent by increasing the recurrence rate RR, but a large recurrence rate RR can present additional issues [39]. We also demonstrated that global ε -recurrence network measures such as transitivity T and the average path length L are more robust at short data lengths compared with other approaches such as the C–E method [3] to distinguish chaos from noise.

We also demonstrated the applicability of the ε -recurrence network measures to the real-world EEG data containing epileptic seizures. Using a small window size (≈ 500 or 1000 samples) and global network measures such as transitivity dimension D_T , assortativity R and average path length L , we were able to capture the rapidly changing dynamics representing pre-seizure, seizure and post-seizure states. The drop in the transitivity dimension D_T and increase in assortativity R and average path length L during the seizure is possibly an indication of a deterministic dynamics and is correlated with increased nonlinearity associated with the seizure activity. These results from observational data provide a useful conclusion that ε -recurrence network measures can successfully detect different states associated with epileptic EEG using rather short window sizes, that can potentially open up some interesting future possibilities in the field of seizure prediction.

Data accessibility. The computations involving recurrence networks were performed using the python package pyunicorn [82] (available at <https://github.com/pik-copan/pyunicorn>). All the other codes to generate simulated data, iAAFT surrogate data, compute C–E plane and recurrence network measures are available at https://github.com/narayan83/RSPA_Codes.

Authors' contributions. N.P.S. is responsible for the initial idea and structure of the paper, which later crystallized over many discussions with J.F.D. N.P.S. designed the simulation section of the paper, analysed the EEG data and interpreted the results, with contributions and comments from J.H. and J.F.D. N.P.S also wrote the paper and the codes to perform the simulations, generate the surrogate data and compute the C–E plane. J.F.D. provided the pyunicorn package used to perform recurrence network-related computations in the work. All the authors gave final approval for publication.

Competing interests. We have no competing interests.

Funding. N.P.S. was supported by the 3DNeuroN project in the European Union's Seventh Framework Programme, Future and Emerging Technologies, (grant agreement no. 296590) and the Tekes Human Spare Parts project. J.F.D. was supported by the Stordalen foundation (via the PB.net initiative) and BMBF (project GLUES).

Acknowledgements. The authors thank the anonymous reviewers for their comments and suggestions, that have helped in improving the quality of the manuscript.

References

1. Marwan N, Donges JF, Zou Y, Donner RV, Kurths J. 2009 Complex network approach for recurrence analysis of time series. *Phys. Lett. A* **373**, 4246–4254. (doi:10.1016/j.physleta.2009.09.042)
2. Zunino L, Soriani MC, Rosso OA. 2012 Distinguishing chaotic and stochastic dynamics from time series by using a multiscale symbolic approach. *Phys. Rev. E* **86**, 046210. (doi:10.1103/PhysRevE.86.046210)
3. Rosso OA, Larrondo HA, Martin MT, Plastino A, Fuentes MA. 2007 Distinguishing noise from chaos. *Phys. Rev. Lett.* **99**, 154102. (doi:10.1103/PhysRevLett.99.154102)
4. Lacasa L, Toral R. 2010 Description of stochastic and chaotic series using visibility graphs. *Phys. Rev. E* **82**, 036120. (doi:10.1103/PhysRevE.82.036120)

5. Kennel MB, Isabelle S. 1992 Method to distinguish possible chaos from colored noise and to determine embedding parameters. *Phys. Rev. A* **46**, 3111–3118. (doi:10.1103/PhysRevA.46.3111)
6. Sugihara G, May RM. 1990 Nonlinear forecasting as a way of distinguishing chaos from measurement error in time series. *Nature* **344**, 734–741. (doi:10.1038/344734a0)
7. Kaplan DT, Glass L. 1992 Direct test for determinism in a time series. *Phys. Rev. Lett.* **68**, 427–430. (doi:10.1103/PhysRevLett.68.427)
8. Kaplan DT, Glass L. 1993 Coarse-grained embeddings of time series: random walks, gaussian random processes, and deterministic chaos. *Physica D: Nonlinear Phenomena* **64**, 431–454. (doi:10.1016/0167-2789(93)90054-5)
9. Osborne AR, Provenzale A. 1989 Finite correlation dimension for stochastic systems with power-law spectra. *Physica D: Nonlinear Phenomena* **35**, 357–381. (doi:10.1016/0167-2789(89)90075-4)
10. Ravetti MG, Carpi LC, Gonçalves BA, Frery AC, Rosso OA. 2014 Distinguishing noise from chaos: objective versus subjective criteria using horizontal visibility graph. *PLoS ONE* **9**, e108004. (doi:10.1371/journal.pone.0108004)
11. Cencini M, Falcioni M, Olbrich E, Kantz H, Vulpiani A. 2000 Chaos or noise: difficulties of a distinction. *Phys. Rev. E* **62**, 427–437. (doi:10.1103/PhysRevE.62.427)
12. Olivares F, Plastino A, Rosso OA. 2012 Ambiguities in Bandt–Pompe’s methodology for local entropic quantifiers. *Physica A: Stat. Mech. Appl.* **391**, 2518–2526. (doi:10.1016/j.physa.2011.12.033)
13. Olivares F, Plastino A, Rosso OA. 2012 Contrasting chaos with noise via local versus global information quantifiers. *Phys. Lett. A* **376**, 1577–1583. (doi:10.1016/j.physleta.2012.03.039)
14. Donner RV, Zou Y, Donges JF, Marwan N, Kurths J. 2010 Recurrence networks—a novel paradigm for nonlinear time series analysis. *N. J. Phys.* **12**, 033025. (doi:10.1088/1367-2630/12/3/033025)
15. Donner RV, Small M, Donges JF, Marwan N, Zou Y, Xiang R, Kurths J. 2011 Recurrence-based time series analysis by means of complex network methods. *Int. J. Bifur. Chaos* **21**, 1019–1046. (doi:10.1142/S0218127411029021)
16. Zhang J, Small M. 2006 Complex network from pseudoperiodic time series: topology versus dynamics. *Phys. Rev. Lett.* **96**, 238701. (doi:10.1103/PhysRevLett.96.238701)
17. Yang Y, Yang H. 2008 Complex network-based time series analysis. *Physica A: Stat. Mech. Appl.* **387**, 1381–1386. (doi:10.1016/j.physa.2007.10.055)
18. Shimada Y, Kimura T, Ikeguchi T. 2008 Analysis of chaotic dynamics using measures of the complex network theory. In *Artificial neural networks - ICANN 2008*, vol. 5163 (eds V Kourková, R Neruda, J Koutník). Lecture Notes in Computer Science, pp. 61–70. Berlin, Germany: Springer.
19. Nicolis G, Cantu AG, Nicolis C. 2005 Dynamical aspects of interaction networks. *Int. J. Bifurcation Chaos* **15**, 3467–3480. (doi:10.1142/S0218127405014167)
20. Donges JF, Donner RV, Kurths J. 2013 Testing time series irreversibility using complex network methods. *Europhys. Lett.* **102**, 10004. (doi:10.1209/0295-5075/102/10004)
21. Lacasa L, Luque B, Ballesteros F, Luque J, Nuño JC. 2008 From time series to complex networks: the visibility graph. *Proc. Natl Acad. Sci. USA* **105**, 4972–4975. (doi:10.1073/pnas.0709247105)
22. Donges JF, Donner RV, Marwan N, Breitenbach SFM, Rehfeld K, Kurths J. 2015 Non-linear regime shifts in holocene Asian monsoon variability: potential impacts on cultural change and migratory patterns. *Clim. Past* **11**, 709–741. (doi:10.5194/cp-11-709-2015)
23. Gao Z-K, Zhang X-W, Jin N-D, Donner RV, Marwan N, Kurths J. 2013 Recurrence networks from multivariate signals for uncovering dynamic transitions of horizontal oil-water stratified flows. *Europhys. Lett.* **103**, 50004. (doi:10.1209/0295-5075/103/50004)
24. Gao Z-K, Yang Y-X, Fang P-C, Zou Y, Xia C-Y, Du M. 2015 Multiscale complex network for analyzing experimental multivariate time series. *Europhys. Lett.* **109**, 30005. (doi:10.1209/0295-5075/109/30005)
25. Gao Z-K, Zhang X-W, Jin N-D, Marwan N, Kurths J. 2013 Multivariate recurrence network analysis for characterizing horizontal oil-water two-phase flow. *Phys. Rev. E* **88**, 032910. (doi:10.1103/PhysRevE.88.032910)
26. Gao Z-K, Yang Y-X, Fang P-C, Jin N-D, Xia C-Y, Hu L-D. 2015 Multi-frequency complex network from time series for uncovering oil-water flow structure. *Sci. Rep.* **5**, 8222. (doi:10.1038/srep08222)

27. Subramaniyam NP, Hyttinen J. 2013 Analysis of nonlinear dynamics of healthy and epileptic eeg signals using recurrence based complex network approach. In *Neural Engineering (NER), 2013 6th Int. IEEE/EMBS Conf., San Diego, CA, 6–8 November*, pp. 605–608. New York, NY: IEEE.
28. Subramaniyam NP, Hyttinen J. 2014 Characterization of dynamical systems under noise using recurrence networks: application to simulated and EEG data. *Phys. Lett. A* **378**, 3464–3474. (doi:10.1016/j.physleta.2014.10.005)
29. Subramaniyam NP, Hyttinen J. 2015 Dynamics of intracranial electroencephalographic recordings from epilepsy patients using univariate and bivariate recurrence networks. *Phys. Rev. E* **91**, 022927. (doi:10.1103/PhysRevE.91.022927)
30. Subramaniyam NP, Hyttinen J, Hatsopoulos NG, Takahashi K. 2015 Recurrence network analysis of wide band oscillations of local field potentials from the primary motor cortex reveals rich dynamics. In *Neural Engineering (NER), 2015 7th Int. IEEE/EMBS Conf., Montpellier, France, 20–24 April*, pp. 960–963. New York, NY: IEEE.
31. Luque B, Lacasa L, Ballesteros F, Luque J. 2009 Horizontal visibility graphs: Exact results for random time series. *Phys. Rev. E* **80**, 046103. (doi:10.1103/PhysRevE.80.046103)
32. Marwan N, Romano MC, Thiel M, Kurths J. 2007 Recurrence plots for the analysis of complex systems. *Phys. Rep.* **438**, 237–329. (doi:10.1016/j.physrep.2006.11.001)
33. Xu X, Zhang J, Small M. 2008 Superfamily phenomena and motifs of networks induced from time series. *Proc. Natl Acad. Sci. USA* **105**, 19601–19605. (doi:10.1073/pnas.0806082105)
34. Eckmann J-P, Kamphorst SO, Ruelle D. 1987 Recurrence plots of dynamical systems. *Europhys. Lett.* **4**, 973–977. (doi:10.1209/0295-5075/4/9/004)
35. Small M, Zhang J, Xu X. 2009 Transforming time series into complex networks. In *Complex sciences*, Lecture Notes of the Institute for Computer Sciences, Social Informatics and Telecommunications Engineering, vol. 5, pp. 2078–2089. Berlin, Heidelberg: Springer.
36. Donges JF, Heitzig J, Donner RV, Kurths J. 2012 Analytical framework for recurrence network analysis of time series. *Phys. Rev. E* **85**, 046105. (doi:10.1103/PhysRevE.85.046105)
37. Zou Y, Donner RV, Donges JF, Marwan N, Kurths J. 2010 Identifying complex periodic windows in continuous-time dynamical systems using recurrence-based methods. *Chaos: An Interdiscip. J. Nonlinear Sci.* **20**, 043130. (doi:10.1063/1.3523304)
38. Dall J, Christensen M. 2002 Random geometric graphs. *Phys. Rev. E* **66**, 016121. (doi:10.1103/PhysRevE.66.016121)
39. Donner RV, Heitzig J, Donges JF, Zou Y, Marwan N, Kurths J. 2011 The geometry of chaotic dynamics—a complex network perspective. *Eur. Phys. J. B-Condensed Matter Complex Syst.* **84**, 653–672. (doi:10.1140/epjb/e2011-10899-1)
40. Schreiber T, Schmitz A. 1996 Improved surrogate data for nonlinearity tests. *Phys. Rev. Lett.* **77**, 635–638. (doi:10.1103/PhysRevLett.77.635)
41. Takens F. 1981 Detecting strange attractors in turbulence. In *Dynamical systems and turbulence, Warwick 1980*, vol. 898 (eds D Rand, L-S Young). Lecture Notes in Mathematics, pp. 366–381. Berlin, Germany: Springer.
42. Kantz H, Schreiber. T. 2004 *Nonlinear time series analysis*, vol. 7. Cambridge, UK: Cambridge University Press.
43. Beauchamp MA. 1965 An improved index of centrality. *Behav. Sci.* **10**, 161–163. (doi:10.1002/bs.3830100205)
44. Sabidussi G. 1966 The centrality index of a graph. *Psychometrika* **31**, 581–603. (doi:10.1007/BF02289527)
45. Scott JP. 2000 *Social network analysis: a handbook*. London, UK: Sage Publications.
46. Wasserman S. 1994 *Social network analysis: methods and applications*, vol. 8. Cambridge, UK: Cambridge University Press.
47. Freeman LC. 1977 A set of measures of centrality based on betweenness. *Sociometry* **40**, 35–41. (doi:10.2307/3033543)
48. Newman MEJ. 2003 The structure and function of complex networks. *SIAM Rev.* **45**, 167–256. (doi:10.1137/S003614450342480)
49. Barrat A, Weigt M. 2000 On the properties of small-world network models. *Eur. Phys. J. B Condensed Matter Complex Syst.* **13**, 547–560. (doi:10.1007/s100510050067)
50. Newman MEJ. 2002 Assortative mixing in networks. *Phys. Rev. Lett.* **89**, 208701. (doi:10.1103/PhysRevLett.89.208701)
51. Boccaletti S, Latora V, Moreno Y, Chavez M, Hwang D-U. 2006 Complex networks: structure and dynamics. *Phys. Rep.* **424**, 175–308. (doi:10.1016/j.physrep.2005.10.009)

52. Donges JF, Donner RV, Rehfeld K, Marwan N, Trauth MH, Kurths J. 2011 Identification of dynamical transitions in marine palaeoclimate records by recurrence network analysis. *Nonlinear Process. Geophys.* **18**, 545–562. (doi:10.5194/npg-18-545-2011)
53. Donges JF, Donner RV, Trauth MH, Marwan N, Schellnhuber H-J, Kurths J. 2011 Nonlinear detection of paleoclimate-variability transitions possibly related to human evolution. *Proc. Natl Acad. Sci. USA* **108**, 20422–20427. (doi:10.1073/pnas.1117052108)
54. Lorenz EN. 1963 Deterministic nonperiodic flow. *J. Atmos. Sci.* **20**, 130–141. (doi:10.1175/1520-0469(1963)020<0130:DNF>2.0.CO;2)
55. Rössler OE. 1976 An equation for continuous chaos. *Phys. Lett. A* **57**, 397–398. (doi:10.1016/0375-9601(76)90101-8)
56. Rossler OE. 1979 An equation for hyperchaos. *Phys. Lett. A* **71**, 155–157. (doi:10.1016/0375-9601(79)90150-6)
57. Fraser AM, Swinney HL. 1986 Independent coordinates for strange attractors from mutual information. *Phys. Rev. A* **33**, 1134–1140. (doi:10.1103/PhysRevA.33.1134)
58. Feldhoff JH, Donner RV, Donges JF, Marwan N, Kurths J. 2012 Geometric detection of coupling directions by means of inter-system recurrence networks. *Phys. Lett. A* **376**, 3504–3513. (doi:10.1016/j.physleta.2012.10.008)
59. Leok M, Tiong B. 1995 Estimating the attractor dimension of the equatorial weather system 1. *Acta Phys. Pol. A* **85**, S27–S35.
60. Zou Y, Donner RV, Wickramasinghe M, Kiss IZ, Small M, Kurths J. 2012 Phase coherence and attractor geometry of chaotic electrochemical oscillators. *Chaos: An Interdiscip. J. Nonlinear Sci.* **22**, 033130. (doi:10.1063/1.4747707)
61. Zhang J, Sun J, Luo X, Zhang K, Nakamura T, Small M. 2008 Characterizing pseudoperiodic time series through the complex network approach. *Physica D: Nonlinear Phenomena* **237**, 2856–2865. (doi:10.1016/j.physd.2008.05.008)
62. Xiang R, Zhang J, Xu X-K, Small M. 2012 Multiscale characterization of recurrence-based phase space networks constructed from time series. *Chaos: An Interdiscip. J. Nonlinear Sci.* **22**, 013107. (doi:10.1063/1.3673789)
63. Donner RV, Zou Y, Donges JF, Marwan N, Kurths J. 2010 Ambiguities in recurrence-based complex network representations of time series. *Phys. Rev. E* **81**, 015101. (doi:10.1103/PhysRevE.81.015101)
64. Zou Y, Heitzig J, Donner RV, Donges JF, Farmer JD, Meucci R, Euzzor S, Marwan N, Kurths J. 2012 Power-laws in recurrence networks from dynamical systems. *Europhys. Lett.* **98**, 48001. (doi:10.1209/0295-5075/98/48001)
65. Rosso OA, Carpi LC, Saco PM, Ravetti MG, Plastino A, Larrondo HA. 2012 Causality and the entropy-complexity plane: Robustness and missing ordinal patterns. *Physica A: Stat. Mech. Appl.* **391**, 42–55. (doi:10.1016/j.physa.2011.07.030)
66. Shannon CE, Weaver W. 1949 *The mathematical theory of communication*. Urbana, IL: University of Illinois Press.
67. Lamberti PW, Martin MT, Plastino A, Rosso OA. 2004 Intensive entropic non-triviality measure. *Physica A: Stat. Mech. Appl.* **334**, 119–131. (doi:10.1016/j.physa.2003.11.005)
68. Bandt C, Pompe B. 2002 Permutation entropy: a natural complexity measure for time series. *Phys. Rev. Lett.* **88**, 174102. (doi:10.1103/PhysRevLett.88.174102)
69. Subramanyam NP, Hyttinen J. 2015 Dynamics of intracranial electroencephalographic recordings from epilepsy patients using univariate and bivariate recurrence networks. *Phys. Rev. E* **91**, 022927. (doi:10.1103/PhysRevE.91.022927)
70. Fisher RS, van Emde Boas W, Blume W, Elger C, Genton P, Lee P, Engel J. 2005 Epileptic seizures and epilepsy: definitions proposed by the International League Against Epilepsy (ILAE) and the International Bureau for Epilepsy (IBE). *Epilepsia* **46**, 470–472. (doi:10.1111/j.1502-9530.2005.66104.x)
71. Quiroga RQ, Blanco S, Rosso OA, Garcia H, Rabinowicz A. 1997 Searching for hidden information with gabor transform in generalized tonic-clonic seizures. *Electroencephalogr. Clin. Neurophysiol.* **103**, 434–439. (doi:10.1016/S0013-4694(97)00031-X)
72. Jasper HH. 1958 The ten twenty electrode system of the international federation. *Electroencephalogr. Clin. Neurophysiol.* **10**, 371–375.
73. Golestani A, Gras R. 2014 Can we predict the unpredictable? *Sci. Rep.* **4**, 6834–6834. (doi:10.1038/srep06834)

74. Wang S, Chaovallitwongse WA, Wong S. 2013 Online seizure prediction using an adaptive learning approach. *IEEE Trans. Knowledge Data Eng.* **25**, 2854–2866. (doi:10.1109/TKDE.2013.151)
75. Stam CJ. 2005 Nonlinear dynamical analysis of EEG and MEG: review of an emerging field. *Clin. Neurophysiol.* **116**, 2266–2301. (doi:10.1016/j.clinph.2005.06.011)
76. Andrzejak RG, Lehnertz K, Mormann F, Rieke C, David P, Elger CE. 2001 Indications of nonlinear deterministic and finite-dimensional structures in time series of brain electrical activity: dependence on recording region and brain state. *Phys. Rev. E* **64**, 061907. (doi:10.1103/PhysRevE.64.061907)
77. Gautama T, Mandic DP, Van Hulle MM. 2004 The delay vector variance method for detecting determinism and nonlinearity in time series. *Physica D: Nonlinear Phenomena* **190**, 167–176. (doi:10.1016/j.physd.2003.11.001)
78. Spencer SS. 2002 Neural networks in human epilepsy: evidence of and implications for treatment. *Epilepsia* **43**, 219–227. (doi:10.1046/j.1528-1157.2002.26901.x)
79. Lemieux L, Daunizeau J, Walker MC. 2011 Concepts of connectivity and human epileptic activity. *Front. Syst. Neurosci.* **5**, 12. (doi:10.3389/fnsys.2011.00012)
80. Friston KJ. 1994 Functional and effective connectivity in neuroimaging: a synthesis. *Hum. Brain Mapp.* **2**, 56–78. (doi:10.1002/hbm.460020107)
81. Donges JF, Schultz HCH, Marwan N, Zou Y, Kurths J. 2011 Investigating the topology of interacting networks. *Eur. Phys. J. B* **84**, 635–651. (doi:10.1140/epjb/e2011-10795-8)
82. Donges JF *et al.* 2015 Unified functional network and nonlinear time series analysis for complex systems science: the pyunicorn package. (<http://arxiv.org/abs/1507.01571>)